Actin reduction by MsrB2 is a key component of the cytokinetic abscission checkpoint and prevents tetraploidy

Jian Bai, Hugo Wioland, Tamara Advedissian, Frédérique Cuvelier, Guillaume Romet - Lemonne, Arnaud Echard

Actin reduction by MsrB2 is a key component of the cytokinetic abscission checkpoint and prevents tetraploidy

Jian Bai[a,b], Hugo Wioland[c], Tamara Advedissian[a], Frédérique Cuvelier[a], Guillaume Romet-Lemonne[c] and Arnaud Echard[a,1]

[a] Membrane Traffic and Cell Division Lab, Institut Pasteur, UMR3691, CNRS, 25-28 rue du Dr Roux, F-75015 Paris, France.

[b] Sorbonne Université, Collège doctoral, F-75005 Paris, France

[c] Institut Jacques Monod, CNRS, Université de Paris, F-75013 Paris, France

[1] To whom correspondence may be addressed. Email: arnaud.echard@pasteur.fr

Abstract

Abscission is the terminal step of cytokinesis leading to the physical separation of the daughter cells. In response to the abnormal presence of lagging chromatin between dividing cells, an evolutionarily-conserved abscission/NoCut checkpoint delays abscission and prevents formation of binucleated cells by stabilizing the cytokinetic intercellular bridge (ICB). How this bridge is stably maintained for hours while the checkpoint is activated is poorly understood and has been proposed to rely on F-actin in the bridge region. Here, we show that actin polymerization is indeed essential for stabilizing the ICB when lagging chromatin is present, but not in normal dividing cells. Mechanistically, we found that a cytosolic pool of human Methionine sulfoxide reductase B2 (MsrB2) is strongly recruited at the midbody in response to the presence of lagging chromatin, and functions within the ICB to promote actin polymerization there. Consistently, in MsrB2-depleted cells, F-actin levels are decreased in ICBs and dividing cells with lagging chromatin become binucleated as a consequence of unstable bridges. We further demonstrate that MsrB2 selectively reduces oxidized actin monomers and thereby counteracts MICAL1, an enzyme known to depolymerize actin filaments by direct oxidation. Finally, MsrB2 colocalizes and genetically interacts with the checkpoint components Aurora B and ANCHR, and the abscission delay upon checkpoint activation by nuclear pore defects also depends on MsrB2. Altogether, this work reveals that actin reduction by MsrB2 is a key component of the abscission checkpoint that favors F-actin polymerization and limits tetraploidy, a starting point for tumorigenesis.

Keywords

actin, cytoskeleton, cytokinesis, oxidoreduction, abscission checkpoint

Significance statement

Cytokinesis concludes cell division by physically separating the daughter cells. Defects in cytokinesis results in tetraploid, binucleated cells that are genetically unstable and represent an important cause of tumorigenesis. The abnormal presence of lagging chromatin within the intercellular bridge (ICB) connecting the daughter cells is detected by an evolutionarily-conserved abscission checkpoint, which delays abscission and stabilizes the ICB for hours, thereby preventing the formation of binucleated cells and DNA damage. Here, we show that the reductase MsrB2 enzymatically controls the polymerization of actin filaments in the ICB and prevents ICB instability specifically in the presence of lagging chromatin. This work thus reveals that actin reduction by MsrB2 is a key component of the abscission checkpoint.

\body

Introduction

The actin cytoskeleton plays a fundamental role in the initial steps of cytokinesis and is essential for cleavage furrow contraction (1-3). The cells are then connected by a thin cytoplasmic canal, the intercellular bridge (ICB) that is eventually cut in a complex process called abscission (4, 5). Abscission occurs on one side of the midbody, the central part of the ICB (6, 7) and relies on ESCRT-III filaments that likely drive the final constriction (8-10). The ESCRT machinery is first recruited at the midbody and later concentrates at the abscission site itself, where the microtubules of the ICB have been cleared by the microtubule-severing enzyme Spastin (11-13). Clearing actin filaments (F-actin) from the ICB is equally important for successful abscission (14). Indeed, the ESCRT-III assembles normally at the midbody but not at the abscission site when actin is not properly depolymerized (14, 15). Two parallel pathways (Rab11/p50RhoGAP and Rab35/OCRL) contribute to prevent excessive actin polymerization in the ICB (5, 16, 17). In addition, we recently found that the Rab35 GTPase recruits the oxidase MICAL1 at the abscission site, in order to clear actin in the ICB (18, 19). MICAL1 belongs to the MICAL monooxygenase family (20-23), directly oxidizes Met44 and Met47 of F-actin into methionine-R-sulfoxides and triggers rapid depolymerization of the

filaments *in vitro* (18, 24-28). Thus, regulated oxidation promotes local F-actin clearance, ESCRT-III recruitment and abscission.

There are nevertheless physiological conditions in which abscission is delayed, notably when the abscission checkpoint / NoCut checkpoint is activated (10, 29-36). This evolutionarily-conserved checkpoint depends on several kinases, including Aurora B, and is triggered by different cytokinetic stresses such as persisting, ultra thin DNA bridges (UFBs) and lagging chromatin positive for nuclear envelop markers (hereafter referred as "chromatin bridges") within the ICB, as well as high membrane tension or nuclear pore defects (32, 37-47). Chromatin bridges spanning between the two daughter nuclei across the ICB can result from DNA replication stress, incomplete DNA decatenation or telomere attrition and activate the checkpoint to delay abscission, presumably giving additional time for resolving these abnormalities (10, 33-35, 48). A defective checkpoint results in cytokinetic failure and binucleated cells (tetraploidy) (32, 38, 44) or chromosome breaks and DNA damage (40, 43, 45-47, 49), and these distinct outcomes apparently depend on which component of the checkpoint has been removed for reasons that are not fully understood (10, 33, 35, 36). In several instances, experimental inactivation of the checkpoint (e.g. Aurora B or ANCHR inactivation), leads to ICB instability and eventually binucleated cells in the presence of chromatin bridges, and to an acceleration of abscission in the absence of chromatin bridges (32, 38, 44, 50). Interestingly, activation of the checkpoint was originally associated with increased F-actin at or close to the ICB, and it was speculated that it could help to maintain ICB stability for hours until chromatin bridges have been resolved (32). More recently, actin patches located at the entry points of the ICBs have been described to depend on the activation of the Src kinase (46) but whether F-actin is essential for the checkpoint has not been directly tested. In addition, little is known about the mechanisms that directly control F-actin levels in the ICB region when the abscission checkpoint is activated.

We hypothesized that oxidation-mediated clearance of F-actin by MICAL1 might be counteracted by actin reduction by Methionine sulfoxide reductases (MsrBs) during cell division. MsrBs belong to a family of enzymes found in all living organisms (51, 52), in particular dSelR in *Drosophila* and its orthologues MsrB1-3 in Humans, that selectively reduce methionine-R-sulfoxide *in vitro* (25, 28, 53). *In vivo, Drosophila* dSelR counteracts dMical-mediated actin disassembly in bristle development, axon guidance and muscle

organization (53). In addition, MsrB1 antagonizes Mical1 and regulates actin-rich processes in stimulated mouse macrophages (25, 28). However, whether MsrBs play a role during cell division is unknown. Here, we report that human MsrB2 controls the timing of abscission, F-actin levels and ICB stability, and plays a critical role to prevent tetraploidy when the abscission checkpoint is activated by lagging chromatin.

Results

Drosophila dSelR and human MsrB2 are negative regulators of cytokinetic abscission

While depletion of dMical delays cytokinetic abscission (18), we now found that depletion of dSelR conversely accelerated abscission in *Drosophila* S2 cells (Supplementary Fig. S1A). Similarly, depletion of MsrB2 accelerated abscission in human HeLa cells (Fig. 1A). Time-lapse phase-contrast microscopy revealed that cell rounding, furrow ingression and ICB formation occurred normally in MsrB2-depleted cells, but the timing of abscission was advanced by approximately 70 min (Fig. 1A and Fig. S1B). The abscission acceleration was fully rescued by expression of an siRNA-resistant version of MsrB2, but not of a catalytically-dead mutant (Fig. 1B and Fig. S1C), indicating that the reductase activity of MsrB2 is critical for controlling the timing of abscission. In contrast, MsrB3 depletion did not perturb the timing of abscission (Fig. S2A). Furthermore, neither the overexpression of MsrB1 nor the overexpression of MsrB3B were able to rescue the accelerated abscission observed in MsrB2-depleted cells (Fig. S2B). Altogether, the Methionine sulfoxide reductases dSelR and MsrB2 play a specific and evolutionarily-conserved role as negative regulators of cytokinetic abscission. In the rest of the manuscript, we focus on human cells to understand how MsrB2 controls abscission and its physiological significance.

MsrB2 counteracts MICAL1-mediated actin oxidation and ESCRT-III recruitment during abscission

To test whether MsrB2 could counteract MICAL1 function during cytokinesis, we compared the timing of abscission in cells depleted for MsrB2, MICAL1 or both (Fig. 1C). MICAL1 depletion delayed abscission by approximately 85 min, as expected (18), whereas co-depletion of MICAL1 and MsrB2 restored normal timing of abscission (Fig. 1C). MICAL1

depletion was previously found to trigger an increase of F-actin in ICBs (Fig. 1D and (18)). In contrast, F-actin levels were diminished in MsrB2-depleted ICBs, compared to controls (Fig. 1D). Interestingly, F-actin levels were restored to normal levels in cells depleted for both MsrB2 and MICAL1 (Fig. 1D). Finally, we previously reported that delayed abscission after MICAL1 depletion was due to defective recruitment of ESCRT-III at the abscission site (18). This is evidenced by a decreased proportion of late ICBs with CHMP4B both at the midbody and abscission site, concomitant with an increased proportion of late ICBs with CHMP4B only at the midbody (Fig. 1E). We observed the opposite phenotype in cells depleted for MsrB2: a decreased proportion of late ICBs with CHMP4B only at the midbody and conversely an increased proportion of late ICBs with CHMP4B both at the midbody and abscission site (Fig. 1E). Remarkably, ESCRT-III localization was as in control cells after co-depletion of MICAL1 and MsrB2 (Fig. 1E). We conclude that MsrB2 counteracts MICAL1 activity in controlling F-actin levels during late cytokinesis, ESCRT-III recruitment at the abscission site and the timing of abscission. Our results also suggest that MsrB2 depletion accelerates abscission by decreasing F-actin levels, which then favors the localization of ESCRT-III at the abscission site.

MsrB2 selectively reduces actin monomers whereas MICAL1 only oxidizes actin filaments *in vitro*

Purified dSelR and MsrB1/B2 are known to counteract MICALs on F-actin polymerization *in vitro*, but this has been documented in bulk, actin-pyrene assays in which the behavior of individual filaments cannot be assayed (25, 28, 53). As such, it is unclear whether MsrB2 acts on MICAL1-oxidized actin filaments and/or on MICAL1-oxidized actin monomers. To address this issue, we took advantage of microfluidics to visualize individual, fluorescently labeled actin filaments, while exposing them successively to different protein solutions. We carried out *in vitro* experiments with the recombinant, active MICAL1 catalytic domain (18) and the active MsrB2 aa 24-182, previously used by others (54). We first subjected F-actin to MICAL1 in order to oxidize the filaments (Fig. 2A, 2B). We then exposed the filaments to buffer and observed the rapid depolymerization of their free barbed ends, approximately 5 times faster than non-oxidized filaments, as expected for oxidized filaments (18, 27) (Fig. 2B). We finally exposed the filaments to MsrB2, along with actin monomers at the critical concentration in order to prevent the filaments from depolymerizing. When

exposing the filaments to buffer again, after exposure to MsrB2, their depolymerization resumed at the same rate as before their exposure to MsrB2 (Fig. 2B). These results indicate that once an actin filament is oxidized, MsrB2 cannot revert its subunits to their initial, slowly depolymerizing state, and show that MsrB2 is unable to act on filaments.

We further investigated how MsrB2 functions by incubating filaments with MICAL1 followed by MsrB2 in bulk, and periodically flowing samples in open chambers for visualization. As expected, addition of MICAL1 catalytic domain led to full depolymerization of actin filaments into monomers after 30 min (Fig. 2C). Remarkably, addition of MsrB2 aa 24-182 (added in excess, since MICAL1 was still present) to the solution of oxidized monomers allowed for the repolymerization of the actin filaments (Fig. 2C). This was not observed if a catalytically-dead version of MsrB2 (C169G, "CD" MsrB2 (55, 56)) was added (Fig. 2A, 2C graph). Interestingly, the core catalytic domain (which is defined as the region highly similar among MsrB1, MsrB2 and MsrB3, aa 75-182, "CC" MsrB2 Fig. 2A) was unable to efficiently restore actin polymerization (Fig. 2C graph), revealing that the N-terminal aa 24-74 of MsrB2 is required for proper actin reduction. We conclude that MsrB2 acts on MICAL1-oxidized monomers and produces reduced actin molecules competent for polymerization into filaments. Conversely, we observed that actin monomers supplemented with profilin (in order to maintain a stable pool of profilin-actin monomers that prevent the spontaneous nucleation of F-actin, as in cells), incubated with the catalytic domain of MICAL1 for up to one hour were still able to polymerize as fast as untreated monomers (Fig. 2D). Thus, MICAL1 does not efficiently oxidize actin monomers, as proposed for *Drosophila* dMical using bulk assays (24). Altogether, our results indicate that MICAL1 acts on actin filaments to induce their oxidation and depolymerization, whereas MsrB2 acts on actin monomers to reduce them and promote their polymerization (Fig. 2E). Therefore, MICAL1 and MsrB2 do not compete for the same substrate, but favor different sides of the actin polymerization/depolymerization cycle, and together modulate actin turnover.

A non-mitochondrial, cytosolic pool of MsrB2 controls the timing of abscission

Human MsrB2 has been previously localized within mitochondria (in the matrix) and the first 23 amino acids are indeed predicted to act as a mitochondrial targeting sequence (MTS) ((54) and Fig. 3A). We thus wondered how MsrB2 could control cytokinetic abscission, since actin monomers reside in the cytosol. Since no antibody specific for MsrB2 is available

for immunofluorescence, we used a C-terminal GFP-fusion MsrB2 (Fig. 3A) to localize MsrB2, as previously described in (54), and we confirmed that the bulk of MsrB2-GFP is localized to mitochondria (Fig. 3B). In addition, we found an unnoticed, diffuse MsrB2 pool within the cytoplasm, detectable in all cells, whatever the level of overexpression (Fig. 3B, insets and Fig. 3C for quantification). This was not an artifact resulting from the saturation of the mitochondrial import machinery, since the mitochondrial matrix marker Mito-dsRed (MTS of cytochrome-c fused to dsRed) co-expressed with MsrB2-GFP was fully localized into mitochondria (Fig. 3B). The MTS of MsrB2 alone (aa 1-23 or MsrB2$^{1-23}$, Fig. 3A), fused to GFP, was localized only in mitochondria in approximately 60% of the cells, and both in the cytosol and mitochondria in the remaining 40% of the cells (Fig. 3C). Interestingly, MsrB2 MTS followed by residues preceding the core catalytic domain (aa 1-74 or MsrB2$^{1-74}$, Fig. 3A) displayed this dual localization in essentially all cells (Fig. 3C). Conversely, a truncated version of MsrB2 lacking the MTS (aa 24-182 or MsrB2$^{24-182}$, Fig. 3A) remained cytosolic (Fig. 3C). These results were confirmed by quantifying the mitochondria:cytosol ratio for the different constructions: MsrB2$^{1-23}$-GFP (MTS alone) localized to mitochondria as much as Tom20's MTS-GFP, whereas MsrB2$^{24-182}$-GFP (lacking the MTS) was cytosolic like GFP alone, and both MsrB2$^{1-74}$-GFP and full length MsrB2-GFP distributed between the cytosol and the mitochondria (Fig. S3A). We conclude that the N-terminal, non-catalytic domain (aa 1-74) is responsible for the localization of MsrB2 in the cytosol, in addition to the mitochondria.

To decide which pool of MsrB2 controls abscission, we measured the timing of abscission in MsrB2-depleted cells that expressed only the cytosolic version of MsrB2 (MsrB2$^{24-182}$ aka Cyto MsrB2, Fig. 3A) and found that it fully restored normal abscission (Fig. 3D and Fig. S3B). In contrast, a cytosolic version of MsrB2 lacking a functional enzymatic activity (Cyto MsrB2$^{Cat\ Dead}$) was unable to rescue the accelerated abscission phenotype resulting from endogenous MsrB2 depletion (Fig. 3E and Fig. S3B). Altogether, our results indicate that the non-mitochondrial pool of MsrB2 is responsible for the control of cytokinetic abscission. This is consistent with the notion that the cytosolic pool of MsrB2 reduces actin in the cytosol, and thus negatively regulates abscission.

MsrB2 depletion leads to binucleated cells in the presence of chromatin bridges

We noticed that a relatively small but reproducible proportion of cells were binucleated after MsrB2 depletion (Fig. 4A). This phenotype was fully rescued by the

expression of a catalytically active (but not a catalytically dead), cytosolic version of MsrB2 (Fig. 4B). However, this phenotype was not significantly rescued by either the expression of catalytically active MsrB1 (p= 0.47, n= 1 004 cells) or MsrB3B (p= 0.98, n= 1 003 cells), reinforcing the idea that among MsrBs, MsrB2 has a specific role in cytokinesis. The modest increase in binucleated cells together with an accelerated abscission observed after MsrB2 depletion prompted us to investigate whether MsrB2 might participate to the abscission checkpoint. Indeed, these two features are observed after inactivation of a subset of checkpoint components (e.g. Aurora B, ANCHR, ALIX), where binucleated cells arise only in the minor proportion of dividing cells harboring abnormal chromatin bridges (32, 38, 44). We thus turned to time-lapse spinning disk confocal microscopy in a cell line that stably expresses a reliable and sensitive marker of chromatin bridges, the nuclear envelope protein LAP2β-GFP (32). When the checkpoint is unperturbed (control RNAi), cells with LAP2β-negative ICBs never became binucleated and only 30% of the cells with LAP2β-positive ICBs became binucleated (Fig. 4C, black bar, Movie S1). These results were in line with previous reports from other labs (32, 44). In contrast, almost all the cells harboring chromatin bridges became binucleated in MsrB2-depleted cells, and this never happened in cells without chromatin bridges (Fig. 4C, red bar, Movie S2). In both control- and MsrB2-depeleted cells, binucleated cells resulted from the regression of the ICB containing a chromatin bridge, approximately 10 hours after complete furrow ingression (Fig. 4C right). Of note, if cells were arrested in cytokinesis by means that did not trigger the abscission checkpoint (i.e. by depleting CEP55), MsrB2 depletion did not destabilize these ICBs (Fig. S3C). The percentage of binucleated cells upon CEP55 and MsrB2 co-depletion was indeed purely additive (Fig. S3C). We conclude that MsrB2 is essential for the normal stabilization of the ICB and to prevent tetraploidy, but only in cells presenting a chromatin bridge. Altogether, our results suggest that MsrB2 is a novel component of the abscission checkpoint.

MsrB2 is recruited to the midbody in the presence of chromatin bridges and controls F-actin levels

We next investigated MsrB2 localization in dividing cells with or without chromatin bridges. In fixed samples, MsrB2 was present as a ring-like structure at the midbody surrounding LAP2β-positive chromatin bridges (57.3% of ICBs, n=96, Fig. 5A left panels). We also sometimes detected MsrB2 in plasma membrane ruffles in the ICB region (23.9% of

ICBs, n=96, Fig. 5A left panels). In dividing cells with no chromatin bridges, MsrB2 was not seen enriched at the midbody or at ruffles (none of 47 ICBs analyzed) (Fig. 5A, right panel). Time-lapse spinning disk confocal microscopy further confirmed that MsrB2-GFP was diffuse and at low levels in the midbody region of dividing cells with no chromatin bridges (22/26 cases) (Fig. S4A, Movie S3), and displayed a more pronounced localization at the midbody in the remaining cases (4/26). Importantly, a strong signal of MsrB2-GFP at the midbody appeared several hours after furrow ingression in the majority of cells presenting a chromatin bridge (9/10 cases, Fig. 5B, Movie S4). Thus, MsrB2 is strongly recruited at the midbody in the presence of chromatin bridges.

We next analyzed the effect of MsrB2 depletion on F-actin among dividing cells presenting a chromatin bridge, using fluorescently-labeled phalloidin. MsrB2 depletion decreased the number of cells with F-actin enrichment in the ICB region (strong F-actin in the ICB and F-actin patches) (Fig. 5C). Quantification further revealed a two-fold decrease of F-actin levels within the intercellular bridge, in the midbody area (Fig. 5D). Of note, MsrB2 depletion did not induce a global decrease of F-actin in the cell bodies (Fig. S4B). Thus, MsrB2 promotes high levels of polymerized F-actin in the presence of chromatin bridges within ICBs and prevents ICB regression when the checkpoint is activated.

Since MsrB2 is strongly recruited at the midbody upon checkpoint activation by lagging chromatin, this ICB-localized pool of MsrB2 might directly reduce actin within the ICBs. Alternatively, the cytosolic pool of MsrB2 outside the ICB might reduce actin in the cell bodies of dividing cells, which could indirectly regulate bridge stability. To decide between these two hypotheses, we investigated whether preventing MsrB2 recruitment to the midbody would rescue the cytokinetic defects observed upon MsrB2 depletion. To this end, we designed an siRNA-resistant version of MsrB2-GFP deleted of its MTS (to prevent its entry into mitochondria, thus identical to Cyto-MsrB2 in Fig. 4B) fused at its N-terminus to the transmembrane domain of the outer mitochondrial membrane protein Tom20 (to immobilize MsrB2 to the cytosolic surface of the mitochondria). The resulting Tom20-ΔMTS MsrB2-GFP (Fig. S4C) was fully retained at the surface of mitochondria and was not recruited to the midbody in dividing cells with lagging chromatin (Fig. 5E, left panels). Remarkably, neither the increase of binucleated cells or the accelerated abscission observed upon MsrB2 depletion were rescued by Tom20-ΔMTS MsrB2-GFP (Fig. 5E, middle and right panels).

Altogether, these results indicate that the localization of MsrB2 at the midbody is key for controlling cytokinetic abscission and bridge stability upon checkpoint activation.

To directly test the importance of actin polymerization in the abscission checkpoint, we recorded cells treated with low doses (20 nM) of LatrunculinA (LatA), a concentration that was chosen to not perturb ICB stability after furrow ingression in normal cells. Indeed, cells with no chromatin bridges did not become binucleated after this LatA treatment (Fig. 5F, Movie S5). In contrast, a strong increase of binucleation, due to ICB regression, was observed in LatA-treated cells that presented a chromatin bridge (Fig. 5F, Movie S6). As after MsrB2 depletion, this happened very late, 9-10 hours after furrow ingression. Altogether, we conclude that appropriate levels of F-actin are crucial for maintaining ICB stability and thus preventing tetraploidization when the abscission checkpoint is activated by lagging chromatin.

MsrB2 colocalizes and genetically interacts with the checkpoint components Aurora B and ANCHR

To further establish that MsrB2 is a component of the abscission checkpoint, we analyzed the relationships between MsrB2 and two core constituents of the checkpoint: Aurora B and ANCHR (32, 38). We first observed that MsrB2 largely colocalized with active, phosphorylated Aurora B at the midbody when the checkpoint was activated by lagging chromatin (Fig. 6A). In addition, the localization of active Aurora B at the midbody did not depend on MsrB2 (Fig. S4D). In previous experiments (Fig. 3D), we noticed that the overexpression of cytosolic MsrB2 by itself was sufficient to delay abscission, presumably because of the higher levels of MsrB2 compared to normal cells. Remarkably, the delay induced by MsrB2 was found to be fully dependent on Aurora B activity (Fig. 6B). Indeed, Aurora B inhibition alone accelerated abscission, as expected (32, 50), and the delay in abscission observed after MsrB2 overexpression was abolished by Aurora B inhibition (Fig. 6B). Aurora B inhibition was actually epistatic to MsrB2 overexpression (Fig. 6B). The fact that Aurora B and MsrB2 genetically interact suggests that they act in the same pathway for regulating abscission.

Similarly, MsrB2 colocalized with ANCHR at the midbody when the checkpoint was activated by lagging chromatin (Fig. 6C). As previously reported (38), ANCHR depletion by itself accelerated abscission (Fig. 6D and S4E). Interestingly, depleting MsrB2 did not

exacerbate this phenotype (Fig. 6D). Furthermore, the percentages of binucleated cells after MsrB2 depletion, ANCHR depletion or co-depletion were identical (Fig. 6D). In addition, MsrB2 promoted ANCHR localization at the midbody in cells with lagging chromatin (Fig. 6E). Altogether, these results are consistent with MsrB2 and ANCHR functioning in the same pathway during cytokinesis and in the checkpoint.

Finally, we tested whether MsrB2 might be important for the abscission checkpoint when it is activated by other means, other than lagging chromatin, such as nuclear pore defects. Partial depletion of the nuclear pore protein Nup153 delays abscission in an Aurora B-dependent manner (37) and we confirmed that it indeed delayed abscission using time-lapse microscopy (Fig. S4F). Interestingly, this delay was significantly attenuated by co-depleting MsrB2 (Fig. S4F). These results indicate that the abscission delay observed when the checkpoint is activated independently of lagging chromatin also depends, at least in part, on MsrB2. Altogether, we propose that MsrB2 is a new component of the abscission checkpoint.

Discussion

We report here the first implication of Methionine Sulfoxide Reductases and more generally of protein reduction in cell division. In the majority of dividing cells (cells without chromatin bridges), MsrB2 acted as a negative regulator of abscission in a reductase-dependent manner (Fig. 1A-C). F-actin intensities at the ICBs and ESCRT-III localization data (Fig. 1D-E) are consistent with the idea that depletion of MsrB2 accelerates abscission by reducing F-actin levels in ICBs, which favors ESCRT-III localization at the abscission site. Since MsrB2 counteracted MICAL1 function during cytokinetic abscission and had opposite effects on F-actin levels in ICBs, ESCRT-III recruitment and timing of abscission, we propose that a balance of actin oxidation by MICAL1 and actin reduction by MsrB2 regulates F-actin polymerization during the terminal steps of cytokinesis. This is evolutionarily-conserved, because dMical depletion (18) and dSelR depletion (this study) had also opposite effects on abscission timing in *Drosophila* cells.

Importantly, MsrB2 depletion led to the formation of binucleated cells in dividing cells with chromatin bridges, but not in normal dividing cells (Fig. 4). This is a phenotype also observed upon inactivation of a subset of core components of the abscission checkpoint,

such as Aurora B, ALIX and ANCHR (32, 38, 44). The colocalization as well as the genetic interactions between MsrB2, Aurora B and ANCHR (Fig. 6A-E) argue that these proteins function in the same pathway. Interestingly, MsrB2 was also involved in delaying abscission in the presence of nuclear pore defects (Fig. S4F), which is a stress that activates the cytokinetic checkpoint independently of chromatin bridges (37). Altogether, our results indicate that MsrB2 represents a novel component of the abscission checkpoint. We notice that MsrB2 and ANCHR displayed strong similarities: their depletion accelerated abscission in normal cells ((38) and Fig. 1), they strongly localized at the midbody in the presence of chromatin bridges ((38) and Fig. 6C), their depletion led to binucleated cells in the presence of chromatin bridges ((38) and Fig. 4), their overexpression delayed abscission in an Aurora B-dependent manner ((38) and Fig. 6B) and their presence contributed to delay abscission upon activation of the checkpoint by nuclear pore defects ((38) and Fig. S4F). Future studies will be required to understand how MsrB2 is recruited at the midbody and how MsrB2/ANCHR together with Aurora B cooperate to prevent tetraploidy in dividing cells with chromatin bridges. Inactivation of other components of the checkpoint can lead to chromosome breaks (40, 43, 45-47, 49), indicating that the checkpoint relies on several branches and is more complex than initially proposed. Nevertheless, we never observed accelerated chromatin bridge resolution or breakage after MsrB2 depletion. Instead, ICBs regressed after approximately 10 hours in the presence of chromatin bridges when MsrB2 is depleted.

The role of F-actin in the stabilization of the ICB when chromatin bridges are present has long been debated (4). To our knowledge, the low-dose LatA experiment reported in Figure 5F is the first direct evidence that actin filaments are indeed important for stabilizing the ICB, selectively when the abscission checkpoint is activated.

In the original report showing that Aurora B is involved in the abscission checkpoint in human cells, it was noticed that actin patches at the entry points of ICBs into the cell bodies were present in dividing cells with chromatin bridges, and this was confirmed by others (32, 46). An important question is to understand whether and how actin patches are implicated in the checkpoint, especially for the integrity of the ICB when chromatin bridges are present. Inhibition of the tyrosine kinase Src has been recently reported to lead to the disappearance of the patches, in correlation with LAP2β-positive bridge breakage and DNA damage (46), arguing that Src could play a role in the abscission checkpoint. However, it

should be pointed out that actin patches are not always seen when chromatin bridges are present in ICBs, and that Src inhibition has strong effects on the overall actin cytoskeleton (57). In addition, the possible role of other pools of F-actin, in particular within ICBs, has not been investigated. Here, we find that MsrB2 depletion reduced the proportion of F-actin-rich ICBs positive for chromatin bridges and decreased F-actin levels at the midbody (Fig. 5C-D). Remarkably, this correlated with an almost systematic destabilization of the ICB, leading to binucleation in cells displaying chromatin bridges (Fig. 4C). We thus propose that the strong recruitment of MsrB2 in chromatin-containing ICBs (Fig. 5A-B) could favor the reduction of actin monomers and thereby promote actin polymerization in the midbody area in order to stabilize the ICBs (Fig. 6F).

We did not observe a global effect on the actin cytoskeleton upon MsrB2 depletion, and cell spreading occurred normally (Fig. S1B). Importantly, a version of MsrB2 that could not localize to the ICB (Tom20-ΔMTS MsrB2-GFP) was unable to rescue the cytokinetic defects (neither accelerated abscission or binucleated cells) observed after depletion of endogenous MsrB2 (Fig. 5E). We thus favor a local and direct role of MsrB2 on actin polymerization and turnover through actin oxidoreduction within the ICB, which appears critical for the stability of ICBs when chromatin bridges are present. Of note, the presence of F-actin promoted by MsrB2 would also contribute to delay abscission by retarding the recruitment of ESCRT-III at the abscission site, since F-actin clearance is necessary for ESCRT-III localization at the abscission site (5, 15-17) (Fig. 6F). This actin-dependent mechanism would act in parallel to other, well-described mechanisms directly acting on the ESCRT machinery, such as CHMP4C, ANCHR and ULK3/IST1 upon checkpoint activation (38, 40, 42, 43).

At the mechanistic level, our *in vitro* experiments revealed that the oxidase MICAL1 and the reductase MsrB2 controlled the amount of F-actin by each targeting separate actin pools. MICAL1 was found to oxidize actin filaments but not actin monomers; conversely, MsrB2 could reduce oxidized monomers but not filaments (Fig. 2). Thus, MICAL1 promotes actin filament depolymerization whereas MsrB2 recycles oxidized monomers into reduced actin molecules competent for polymerization (Fig. 2E). Interestingly, the N-terminal part of MsrB2 (aa 24-74), which precedes the catalytic domain, appeared to play a critical role for actin reduction (Fig. 2C, compare MsrB2 aa 24-182 vs. CC MsrB2). It could potentially activate the enzymatic activity of the core catalytic domain (aa 75-182) or alternatively

promote actin binding to the enzyme. Crystallographic data show that the unusually extended N-terminus of MsrB2 is structurally distinct from the enzymatic domain, and our results are consistent with the hypothesis that it could play a role in substrate specificity or affinity (58).

The N-terminus domain of MsrB2 plays also a critical role for its subcellular localization. MsrB2 was previously reported to localize to mitochondria (54). We confirmed this localization and describe here an additional, cytosolic pool that depended on the domain preceding the core enzymatic domain (Fig. 3). We found that aa 1-23 acted as a mitochondrial targeting signal, and that aa 24-74 were key for the retention of MsrB2 into the cytosol. It is conceivable that the latter region partially masks the MTS or interacts with yet-to-be-discovered cytosolic proteins that retain a fraction of MsrB2 outside mitochondria. This is not unique to MsrB2, since a number of mitochondrial proteins have been described to localize outside mitochondria as well (59). Importantly, our results argue that the cytosolic pool of MsrB2, but not the mitochondrial one, is critical for the control of abscission (Fig. 3D-E). Of note, MsrB1 and MsrB3 were reported to be cytosolic and/or associate to the ER and we did not find evidence that they were implicated in cytokinesis (Fig. S2), suggesting that MsrBs exert non-overlapping functions in human cells.

In conclusion, the Methionine sulfoxide reductase MsrB2 represents a novel component of the abscission checkpoint, and prevents the formation of genetically unstable, tetraploid cells (Fig. 6F). This work also reveals a direct role of the actin cytoskeleton in the abscission checkpoint and highlights the importance of targeted actin reduction in cell physiology.

Materials and methods

Detailed experimental procedures and data analysis used in this study are described in SI Appendix, Supplementary Methods and Information.

Cell cultures

Drosophila Anillin-mCherry S2 cell line was generated and characterized in (60) (kind gift from Dr Gilles Hickson, St Justin, Montréal) and grown in Schneider medium (Invitrogen) at 26°C. HeLa cells cl2 from the ATCC were grown in Dulbecco's Modified Eagle Medium (DMEM) GlutaMax (31966; Gibco, Invitrogen Life Technologies) supplemented with 10% fetal bovine serum (FBS) and 1% Penicillin-Streptomycin (Gibco) in 5% CO2 condition at 37°C. HeLa LAP2β-GFP + H2B-RFP and Actin-GFP + LAP2β-RFP stable cell lines have been characterized in (32) (kind gifts from Dr Daniel Gerlich, IMBA, Vienna), and were cultured in DMEM with 10% FBS, 0.5 µg/ml puromycin and 0.5 mg/ml G418. For LatrunculinA experiments, Actin-GFP + LAP2β-RFP HeLa cells were treated with 20 nM LatrunculinA (Sigma-Aldrich).

Data Availability Statement: All data discussed in the paper will be made available to readers.

Acknowledgments

We thank the Echard Lab members, T. Wai and I. Petropoulos for helpful discussions and reagents. We thank the imaging facilities Utechs PBI, Institut Pasteur and PH Commere of the Cytometry Utechs, Institut Pasteur. Work in the Echard Lab has been supported by Institut Pasteur, CNRS, and ANR (AbsCystem and RedoxActin). J.B. was supported by the Pasteur-Paris University (PPU) international PhD program, and received a fellowship from Fondation ARC pour la recherche sur le cancer (DOC20180507410). H.W. has been supported by a postdoctoral fellowship from the Fondation ARC pour la recherche sur le cancer. T. A. has been supported by a postdoctoral fellowship from the Fondation pour la Recherche Médicale (FRM # SPF201809006907) and the ANR (Cytosign).

The authors declare no competing financial interests.

Author contributions

J.B. designed, carried out and analyzed the experiments presented in Fig. 1, 3, 4, 5, 6A, 6D, 6E, S1, S2, S3B, S3C and S4; H.W. in Fig. 2; T.A. in Fig. 6B, 6C and S3A. F.C. assisted with technical help. A.E. conceived the project and secured funding. A.E. supervised the cell biology data; G.R-L. supervised the *in vitro* data. A.E. and G.R-L. wrote the manuscript with the help of J.B., H.W and T.A.

References

1. Green RA, Paluch E, & Oegema K (2012) Cytokinesis in Animal Cells. *Annual review of cell and developmental biology*.
2. D'Avino PP, Giansanti MG, & Petronczki M (2015) Cytokinesis in animal cells. *Cold Spring Harbor perspectives in biology* 7(4):a015834.
3. Pollard TD (2017) Nine unanswered questions about cytokinesis. *The Journal of cell biology* 216(10):3007-3016.
4. Mierzwa B & Gerlich DW (2014) Cytokinetic Abscission: Molecular Mechanisms and Temporal Control. *Developmental cell* 31(5):525-538.
5. Fremont S & Echard A (2018) Membrane Traffic in the Late Steps of Cytokinesis. *Current biology : CB* 28(8):R458-R470.
6. Dionne LK, Wang XJ, & Prekeris R (2015) Midbody: from cellular junk to regulator of cell polarity and cell fate. *Current opinion in cell biology* 35:51-58.
7. Crowell EF, Gaffuri AL, Gayraud-Morel B, Tajbakhsh S, & Echard A (2014) Midbody remnant engulfment after cytokinesis abscission in mammalian cells. *J Cell Sci* 127(17):3840-3851.
8. Carlton JG & Martin-Serrano J (2007) Parallels between cytokinesis and retroviral budding: a role for the ESCRT machinery. *Science* 316(5833):1908-1912.
9. Morita E*, et al.* (2007) Human ESCRT and ALIX proteins interact with proteins of the midbody and function in cytokinesis. *The EMBO journal* 26(19):4215-4227.
10. Stoten CL & Carlton JG (2017) ESCRT-dependent control of membrane remodelling during cell division. *Seminars in cell & developmental biology*.
11. Connell JW, Lindon C, Luzio JP, & Reid E (2009) Spastin couples microtubule severing to membrane traffic in completion of cytokinesis and secretion. *Traffic* 10(1):42-56.
12. Schiel JA*, et al.* (2011) Endocytic membrane fusion and buckling-induced microtubule severing mediate cell abscission. *J Cell Sci* 124(Pt 9):1411-1424.
13. Lafaurie-Janvore J*, et al.* (2013) ESCRT-III assembly and cytokinetic abscission are induced by tension release in the intercellular bridge. *Science* 339(6127):1625-1629.
14. Addi C, Bai J, & Echard A (2018) Actin, microtubule, septin and ESCRT filament remodeling during late steps of cytokinesis. *Current opinion in cell biology* 50:27-34.
15. Terry SJ, Dona F, Osenberg P, Carlton JG, & Eggert US (2018) Capping protein regulates actin dynamics during cytokinetic midbody maturation. *Proceedings of the National Academy of Sciences of the United States of America* 115(9):2138-2143.
16. Dambournet D*, et al.* (2011) Rab35 GTPase and OCRL phosphatase remodel lipids and F-actin for successful cytokinesis. *Nature cell biology* 13(8):981-988.
17. Schiel JA*, et al.* (2012) FIP3-endosome-dependent formation of the secondary ingression mediates ESCRT-III recruitment during cytokinesis. *Nature cell biology* 14:1068-1078.
18. Fremont S*, et al.* (2017) Oxidation of F-actin controls the terminal steps of cytokinesis. *Nat Commun* 8:14528.
19. Klinkert K & Echard A (2016) Rab35 GTPase: a central regulator of phosphoinositides and F-actin in endocytic recycling and beyond. *Traffic*.
20. Alto LT & Terman JR (2018) MICALs. *Current biology : CB* 28(9):R538-R541.

21. Fremont S, Romet-Lemonne G, Houdusse A, & Echard A (2017) Emerging roles of MICAL family proteins - from actin oxidation to membrane trafficking during cytokinesis. *J Cell Sci* 130(9):1509-1517.
22. Manta B & Gladyshev VN (2017) Regulated methionine oxidation by monooxygenases. *Free radical biology & medicine* 109:141-155.
23. Giridharan SS & Caplan S (2013) MICAL-Family Proteins: Complex Regulators of the Actin Cytoskeleton. *Antioxid Redox Signal*.
24. Hung RJ, Pak CW, & Terman JR (2011) Direct redox regulation of F-actin assembly and disassembly by Mical. *Science* 334(6063):1710-1713.
25. Lee BC*, et al.* (2013) MsrB1 and MICALs regulate actin assembly and macrophage function via reversible stereoselective methionine oxidation. *Mol Cell* 51(3):397-404.
26. Lundquist MR*, et al.* (2014) Redox modification of nuclear actin by MICAL-2 regulates SRF signaling. *Cell* 156(3):563-576.
27. Grintsevich EE*, et al.* (2017) Catastrophic disassembly of actin filaments via Mical-mediated oxidation. *Nat Commun* 8(1):2183.
28. Wu H, Yesilyurt HG, Yoon J, & Terman JR (2018) The MICALs are a Family of F-actin Dismantling Oxidoreductases Conserved from Drosophila to Humans. *Scientific reports* 8(1):937.
29. Mendoza M*, et al.* (2009) A mechanism for chromosome segregation sensing by the NoCut checkpoint. *Nature cell biology* 11(4):477-483.
30. Norden C*, et al.* (2006) The NoCut pathway links completion of cytokinesis to spindle midzone function to prevent chromosome breakage. *Cell* 125(1):85-98.
31. Amaral N*, et al.* (2016) The Aurora-B-dependent NoCut checkpoint prevents damage of anaphase bridges after DNA replication stress. *Nature cell biology* 18(5):516-526.
32. Steigemann P*, et al.* (2009) Aurora B-mediated abscission checkpoint protects against tetraploidization. *Cell* 136(3):473-484.
33. Nahse V, Christ L, Stenmark H, & Campsteijn C (2017) The Abscission Checkpoint: Making It to the Final Cut. *Trends in cell biology* 27(1):1-11.
34. Agromayor M & Martin-Serrano J (2013) Knowing when to cut and run: mechanisms that control cytokinetic abscission. *Trends in cell biology* 23(9):433-441.
35. Lens SMA & Medema RH (2019) Cytokinesis defects and cancer. *Nature reviews. Cancer* 19(1):32-45.
36. Petsalaki E & Zachos G (2019) Building bridges between chromosomes: novel insights into the abscission checkpoint. *Cellular and molecular life sciences : CMLS* 76(21):4291-4307.
37. Mackay DR, Makise M, & Ullman KS (2010) Defects in nuclear pore assembly lead to activation of an Aurora B-mediated abscission checkpoint. *The Journal of cell biology* 191(5):923-931.
38. Thoresen SB*, et al.* (2014) ANCHR mediates Aurora-B-dependent abscission checkpoint control through retention of VPS4. *Nature cell biology*.
39. Mackay DR & Ullman KS (2015) ATR and a Chk1-Aurora B pathway coordinate postmitotic genome surveillance with cytokinetic abscission. *Molecular biology of the cell* 26(12):2217-2226.
40. Carlton JG, Caballe A, Agromayor M, Kloc M, & Martin-Serrano J (2012) ESCRT-III governs the Aurora B-mediated abscission checkpoint through CHMP4C. *Science* 336(6078):220-225.

41. Capalbo L*, et al.* (2016) Coordinated regulation of the ESCRT-III component CHMP4C by the chromosomal passenger complex and centralspindlin during cytokinesis. *Open biology* 6(10).
42. Capalbo L*, et al.* (2012) The chromosomal passenger complex controls the function of endosomal sorting complex required for transport-III Snf7 proteins during cytokinesis. *Open biology* 2(5):120070.
43. Caballe A*, et al.* (2015) ULK3 regulates cytokinetic abscission by phosphorylating ESCRT-III proteins. *eLife* 4:e06547.
44. Christ L*, et al.* (2016) ALIX and ESCRT-I/II function as parallel ESCRT-III recruiters in cytokinetic abscission. *The Journal of cell biology* 212(5):499-513.
45. Petsalaki E & Zachos G (2016) Clks 1, 2 and 4 prevent chromatin breakage by regulating the Aurora B-dependent abscission checkpoint. *Nat Commun* 7:11451.
46. Dandoulaki M, Petsalaki E, Sumpton D, Zanivan S, & Zachos G (2018) Src activation by Chk1 promotes actin patch formation and prevents chromatin bridge breakage in cytokinesis. *The Journal of cell biology* 217(9):3071-3089.
47. Bhowmick R*, et al.* (2019) The RIF1-PP1 Axis Controls Abscission Timing in Human Cells. *Current biology : CB* 29(7):1232-1242 e1235.
48. Hong Y*, et al.* (2018) LEM-3 is a midbody-tethered DNA nuclease that resolves chromatin bridges during late mitosis. *Nat Commun* 9(1):728.
49. Sadler JBA*, et al.* (2018) A cancer-associated polymorphism in ESCRT-III disrupts the abscission checkpoint and promotes genome instability. *Proceedings of the National Academy of Sciences of the United States of America* 115(38):E8900-E8908.
50. Mathieu J*, et al.* (2013) Aurora B and cyclin B have opposite effects on the timing of cytokinesis abscission in Drosophila germ cells and in vertebrate somatic cells. *Developmental cell* 26(3):250-265.
51. Tarrago L & Gladyshev VN (2012) Recharging oxidative protein repair: catalysis by methionine sulfoxide reductases towards their amino acid, protein, and model substrates. *Biochemistry. Biokhimiia* 77(10):1097-1107.
52. Achilli C, Ciana A, & Minetti G (2015) The discovery of methionine sulfoxide reductase enzymes: An historical account and future perspectives. *BioFactors* 41(3):135-152.
53. Hung RJ, Spaeth CS, Yesilyurt HG, & Terman JR (2013) SelR reverses Mical-mediated oxidation of actin to regulate F-actin dynamics. *Nature cell biology* 15(12):1445-1454.
54. Kim HY & Gladyshev VN (2004) Methionine sulfoxide reduction in mammals: characterization of methionine-R-sulfoxide reductases. *Molecular biology of the cell* 15(3):1055-1064.
55. Jung S, Hansel A, Kasperczyk H, Hoshi T, & Heinemann SH (2002) Activity, tissue distribution and site-directed mutagenesis of a human peptide methionine sulfoxide reductase of type B: hCBS1. *FEBS letters* 527(1-3):91-94.
56. Kim HY & Gladyshev VN (2005) Different catalytic mechanisms in mammalian selenocysteine- and cysteine-containing methionine-R-sulfoxide reductases. *PLoS biology* 3(12):e375.
57. Bursell L*, et al.* (2007) Src kinase inhibition promotes the chondrocyte phenotype. *Arthritis Res Ther* 9(5):R105.
58. Aachmann FL*, et al.* (2011) Structural and biochemical analysis of mammalian methionine sulfoxide reductase B2. *Proteins* 79(11):3123-3131.
59. Dinur-Mills M, Tal M, & Pines O (2008) Dual targeted mitochondrial proteins are characterized by lower MTS parameters and total net charge. *PloS one* 3(5):e2161.

60. El Amine N, Kechad A, Jananji S, & Hickson GR (2013) Opposing actions of septins and Sticky on Anillin promote the transition from contractile to midbody ring. *The Journal of cell biology* 203(3):487-504.

Figure Legends

Figure 1: MsrB2 is a negative regulator of cytokinetic abscission and counteracts MICAL1-mediated actin oxidation and ESCRT-III recruitment.

(A) Left: lysates from HeLa cells treated with control or MsrB2 siRNAs were blotted for MsrB2 and β-tubulin (loading control). Middle and Right: distribution of the abscission time (p< 0.001, non-parametric and distribution-free Kolmogorov–Smirnov KS test) and mean abscission time ± SD in control- and MsrB2-depleted cells (N=3). n=244-247 cells per condition. *(B)* Distribution of abscission time (Left and Middle) and mean abscission time ± SD (Right) for control- and MsrB2-depleted cells transfected with indicated plasmids (N=3). n=217-227 cells per condition. No statistical difference between black and either green, blue or grey curves. No statistical difference between red and yellow curve. p= 0.001 between black and either red or yellow curves (KS test). n=217-227 cells per condition. *(C)* Left: lysates from cells treated with control, MsrB2, MICAL1 or MsrB2+MICAL1 siRNAs were blotted for MICAL1, MsrB2 and β-tubulin (loading control). Middle and Right: distribution of the abscission time and mean abscission time ± SD for the same cell populations described in the left panel (N=3). n=233-245 cells per condition. No statistical significance between black and blue curves, p< 0.001 between black and red curve, p= 0.066 between black and green curve (KS test). *(D)* F-actin intensity in the ICBs from the same cell populations used in *(C)* (N=3). n=64-89 ICBs per condition. Mean ± SD. Bottom: representative images of F-actin in the ICBs for the corresponding conditions. Scale bar: 2 µm. *(E)* Quantification of ICBs with either No CHMP4B (bottom left image), with CHMP4B only at the midbody (bottom middle image) or with CHMP4B both at midbody and abscission site (bottom right image) for each cell population described in *(C)* (N=3). n=151-153 ICBs per condition. Mean ± SD. Brackets and arrowhead mark the midbody and the abscission site, respectively. Scale bar: 2 µm. NS, not significant. p values (Student-t tests) are indicated.

Figure 2: MsrB2 selectively reduces actin monomers whereas MICAL1 only oxidizes actin filaments *in vitro.*

(A) MICAL1 and MsrB2 constructs used in this Figure. aa: amino acid. *(B)* MsrB2 aa 24-182 cannot reduce F-actin. Upper panels: time-lapse of the depolymerization of a single filament oxidized by MICAL1, sequentially exposed to buffer (a phase during which the filament

depolymerized) and MsrB2 aa 24-182 (supplemented with actin at its critical concentration, 0.1 µM, such as the filament length remained constant during this phase). Lower panel: the barbed end (BE) depolymerization rate is constant despite exposing the filament to MsrB2 aa 24-182. The depolymerization rates are normalized by the average depolymerization rate of oxidized filaments that have not been exposed to MsrB2 aa 24-182. N=30 filaments, points: mean ± SD. *(C)* MsrB2 aa 24-182, but not a catalytically dead mutant (CD) or its catalytic core domain (CC), can reduce MICAL1-oxidized G-actin to allow repolymerization. Upper panel: sketch of the procedure and typical fields of view (cropped): 2 µM F-actin are sequentially incubated with MICAL1 (or buffer, for 90 minutes) and MrB2 constructs (or buffer, for various times). Fractions of this solution are diluted 20-fold into F-buffer supplemented with 0.3% methylcellulose and injected into an open chamber for visualization. Lower panel: quantification of the density of actin filaments. For each experiment and time point, we measured the total F-actin length in 4 to 12 individual fields of view, 10 000 µm² each. Points: 1 to 4 independent experiments, mean ± SD. *(D)* MICAL1 does not oxidize G-actin. Upper panels: time-lapse images showing barbed end polymerization from a solution of profilin-actin containing NADPH, with or without MICAL1, incubated for up to 60 min, prior to elongation (the 0.6 µM actin solution was supplemented with 1 µM profilin to prevent spontaneous nucleation and to maintain a stable pool of G-actin). Lower panel: polymerization rate is independent of incubation time and presence of MICAL1. N = 20 filaments (2 experiments), points: mean ± SD. *(E)* Regulation of actin turnover by the MICAL1/MsrB2 redox balance: MICAL1 oxidizes actin filaments, driving their depolymerization and the formation of oxidized monomers, while MsrB2 reduces the oxidized monomers, allowing them to repolymerize into filaments.

Figure 3: MsrB2 localizes to both mitochondria and cytosol and the cytosolic pool of MsrB2 controls the timing of abscission.

(A) MsrB2 constructs used in this study. MTS: mitochondrial targeting sequence; GFP: Green Fluorescence Protein; aa: amino acid; Cyto: cytosolic. *(B)* Top: cells expressing MsrB2-GFP (green) were stained with Tom22 (red). Bottom: cells co-expressing MsrB2-GFP (green) and Mito-dsRed (red). Scale bar: 10 µm. *(C)* Upper panels: cells expressing MsrB2 MTS-GFP (top, green) or MsrB2 aa 1-74-GFP (middle, green) or MsrB2 aa 24-182-GFP (bottom, green) were stained with Tom22 (red). Scale bar: 10 µm. Lower panel: percentage of MsrB2-GFP, MsrB2

MTS-GFP, MsrB2 aa 1-74-GFP or MsrB2 aa 24-182-GFP transfected cells displaying both mitochondria and cytosol localization (*N*=3). *n*=1500 cells per condition. *(D, E)* Distribution of the abscission time and mean abscission time ± SD in control- and MsrB2-depleted cells transfected with indicated plasmids (*N*=3). *n*=171-224 cells per condition. In *(D)*: No statistical significance between black and blue curves, *p*< 0.001 between black and red curves, *p*= 0.014 between black and green curves (KS test). In *(E)*: No statistical significance between black and green curves, or red and blue curves, *p*< 0.001 between black and either red or blue curves (KS test). NS, not significant. p values (Student-t tests) are indicated.

Figure 4: MsrB2 depletion leads to binucleated cells exclusively in the presence of chromatin bridges.

(A) Left: control- and MsrB2-depleted cells were stained with DAPI (blue) and Acetylated-tubulin (green). White arrows indicate multinucleated cells. Scale bar: 20 µm. Right: percentage of multinucleated cells after control or MsrB2 depletion (*N*=3). n=1500 cells per condition. Mean ± SD. *(B)* Percentage of multinucleated cells after control or MsrB2 depletion and transfection with indicated plasmids (*N*=3). n=1500 cells per condition. Mean ± SD. *(C)* Left: snapshot of time-lapse spinning-disk confocal microscopy movies of LAP2β-GFP cells treated with either control or MsrB2 siRNAs. Green stars and green arrowheads mark metaphase cells and chromatin bridges, respectively. Scale bar: 5 µm. Middle: percentage of dividing control- and MsrB2-depleted cells without (left box) or with (right box) chromatin bridges that eventually became binucleated (*N=3*). n=860-946 cell divisions per condition. Right: time from completion of furrow ingression to ICB regression in control- and MsrB2-depleted cells displaying chromatin bridges (*N*=3). n=41-78 cells per condition. Mean ± SD. NS, not significant. p values (Student-t tests) are indicated.

Figure 5: MsrB2 is recruited to the midbody in the presence of chromatin bridges and controls F-actin levels.

(A) Cells expressing MsrB2-GFP (green) were stained with LAP2β (red) and Acetyl-tubulin (blue). Indicated zoomed regions are also presented (lower panels). The Acetyl-tubulin channel has been displayed only for the ICB with no chromatin bridge (right panel). Scale bar: 10 µm. *(B)* Snapshots of a time-lapse spinning-disk confocal microscopy movie of cells expressing MsrB2-GFP (green) and LAP2β-RFP (red), labeled with SiR-tubulin (blue). Green

arrowheads indicate chromatin bridges. Scale bar: 10 µm. *(C)* Left: representative images of cells stained with phalloidin (green) and LAP2β (red). White arrowheads indicate chromatin bridges. Scale bar: 10 µm. Right: percentage of control- and MsrB2-depleted cells with LAP2β-positive chromatin bridges with F-actin enrichment in the ICB region (*N*=3). n=114-115 chromatin bridges containing ICBs. Mean ± SD. *(D)* Left: representative images of control- and MsrB2-depleted cells stained with phalloidin (green), LAP2β (red) and Ac-tubulin (blue). Right: quantification of F-actin intensity in the midbody region (brackets) in control- or MsrB2-depleted cells with LAP2β positive chromatin bridges (*N*=3). n=21-30 chromatin bridges-positive ICBs per condition. Mean ± SD. *(E)* Left: representative images of cells expressing Tom20$^{1-35}$-GFP (green, upper panel) or Tom20$^{1-35}$-ΔMTS MsrB2-GFP (green, bottom panel) stained with LAP2β (red). Scale bar: 10 µm. Middle: distribution of abscission time and mean abscission time ± SD for control- and MsrB2-depleted cells transfected with indicated plasmids (*N*=3). n=226-240 cells per condition. No statistical difference between black and green curves or between red and blue curves. *p*= 0.001 between black and red curves (KS test). Right: percentage of multinucleated cells after control or MsrB2 depletion and transfection with indicated plasmids (*N*=3). n=1500 cells per condition. Mean ± SD. *(F)* Left: percentage of dividing cells without (left box) or with (right box) chromatin bridges that became binucleated after treatment with either DMSO or 20nM LatA (*N=3*). n=485-555 cell division per condition. Right: time from completion of furrow ingression to ICB regression in DMSO- or 20 nM LatA-treated cells displaying chromatin bridges (*N*=3). n=15-31 cells per condition. Mean ± SD. NS, not significant. p values (Student-t tests) are indicated.

Figure 6: MsrB2 colocalizes and genetically interacts with Aurora B and ANCHR

(A) Cells expressing MsrB2-GFP (green) were stained with p-Aurora B (red) and LAP2β (grey, insert). Merged zoom of the midbody and individual red/green channels are also displayed, as indicated. Scale bar: 10 µm. *(B)* distribution of abscission time (left) and mean abscission time ± SD (right) for GFP or Cyto MsrB2-GFP-expressing cells treated with either DMSO or Aurora B inhibitor ZM447439 (*N*=3). n=93-99 cells per condition. *p*= 0.035 between black and green curves. *p*= 0.038 between black and red curves. No statistical difference between green and blue curves (KS tests). *(C)* Cells expressing GFP-ANCHR and MsrB2-mCherry were stained with LAP2β (grey, insert). Merged zoom of the midbody and individual red/green channels are also displayed, as indicated. Scale bar: 10 µm. *(D)* Distribution of abscission

time (left) and mean abscission time ± SD (middle) for control, MsrB2, ANCHR or MsrB2+ANCHR depleted cells (N=3). n=241-247 cells per condition. $p< 0.001$ between black and either red, green or blue curves. No statistical difference between red, green and blue curves (KS tests). Right: percentage of multinucleated cells after control, MsrB2, ANCHR or MsrB2+ANCHR depletion (*N*=3). n=1500 cells per condition. Mean ± SD *(E)* Left: representative images of control and MsrB2-depleted cells stained for endogenous ANCHR (green) and LAP2β (red). Inserts correspond to the indicated zoomed regions (midbodies). Scale bar: 10 µm. Right: triplicate quantification for mean ANCHR fluorescent intensity (arbitrary units) in the midbodies of control- and MsrB2-depleted cells in the presence of LAP2β-positive chromatin bridges. n=63-68 midbodies per condition. *(F)* Model: The reduction of G-actin by MsrB2 regulates its polymerization cycle by countering the effect of oxidation by MICAL1, thereby favoring the polymerization of actin filaments in the ICB. This F-actin pool delays the recruitment of ESCRT-III at the abscission site, and stabilizes the ICB when a chromatin bridge is present. ICB: intercellular bridge. A green arrow means 'favors' and a red arrow means 'inhibits' localization and/or activity, whether the effect is direct or indirect. NS, not significant. p values (Student-t tests) are indicated.

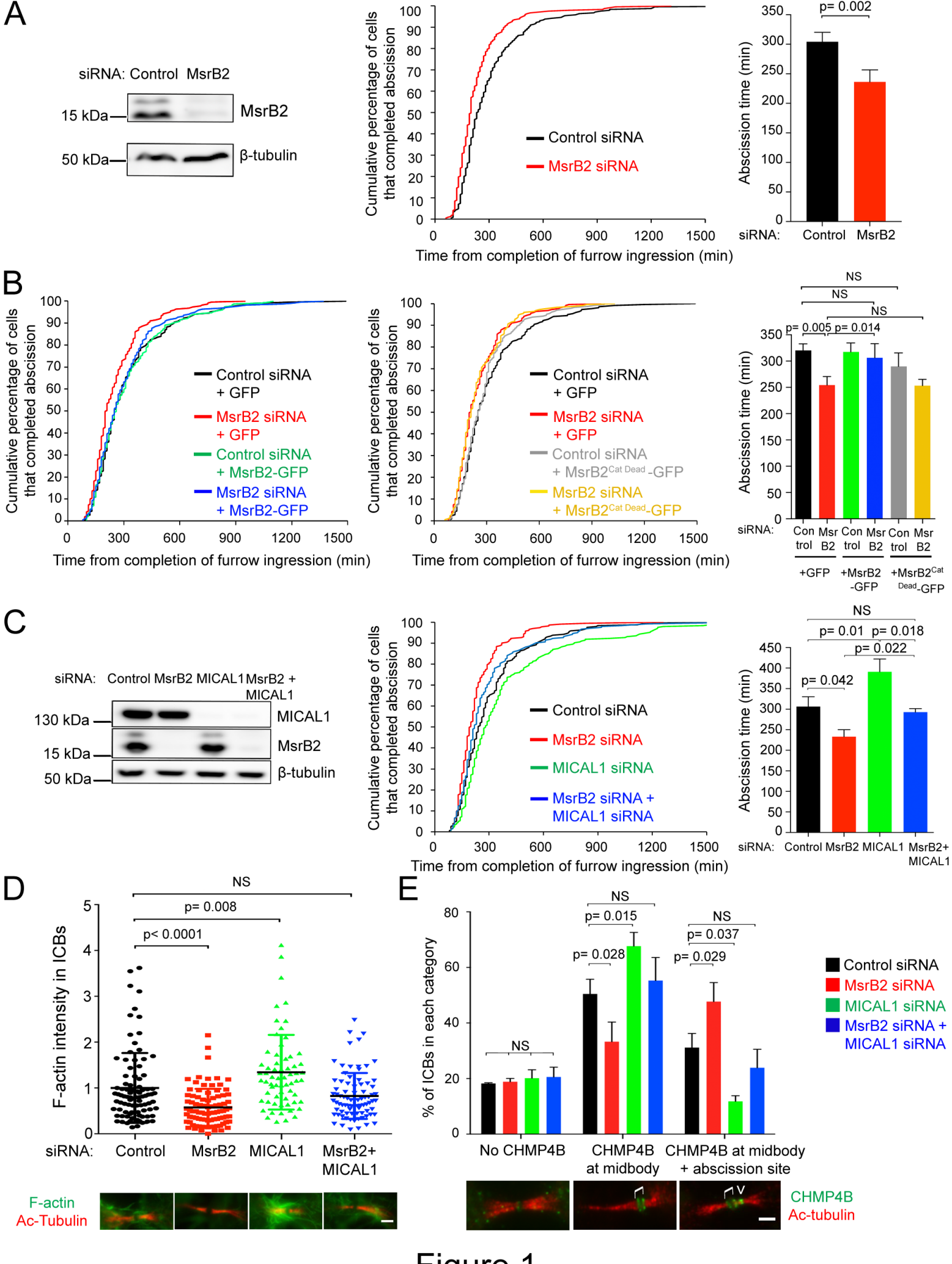
A
siRNA: Control MsrB2
15 kDa
MsrB2
50 kDa
β-tubulin
Cumulative percentage of cells that completed abscission
Control siRNA
MsrB2 siRNA
Time from completion of furrow ingression (min)
p= 0.002
Abscission time (min)
siRNA: Control MsrB2
B
Control siRNA + GFP
MsrB2 siRNA + GFP
Control siRNA + MsrB2-GFP
MsrB2 siRNA + MsrB2-GFP
Control siRNA + MsrB2Cat Dead-GFP
MsrB2 siRNA + MsrB2Cat Dead-GFP
NS
p= 0.005
p= 0.014
Control
MsrB2
+GFP
+MsrB2-GFP
+MsrB2Cat Dead-GFP
C
siRNA: Control MsrB2 MICAL1 MsrB2 + MICAL1
130 kDa
MICAL1
15 kDa
MsrB2
50 kDa
β-tubulin
Control siRNA
MsrB2 siRNA
MICAL1 siRNA
MsrB2 siRNA + MICAL1 siRNA
p= 0.01
p= 0.018
p= 0.022
p= 0.042
D
F-actin intensity in ICBs
p< 0.0001
p= 0.008
siRNA: Control MsrB2 MICAL1 MsrB2+ MICAL1
F-actin
Ac-Tubulin
E
% of ICBs in each category
p= 0.028
p= 0.015
p= 0.029
p= 0.037
No CHMP4B
CHMP4B at midbody
CHMP4B at midbody + abscission site
CHMP4B
Ac-tubulin

Figure 1

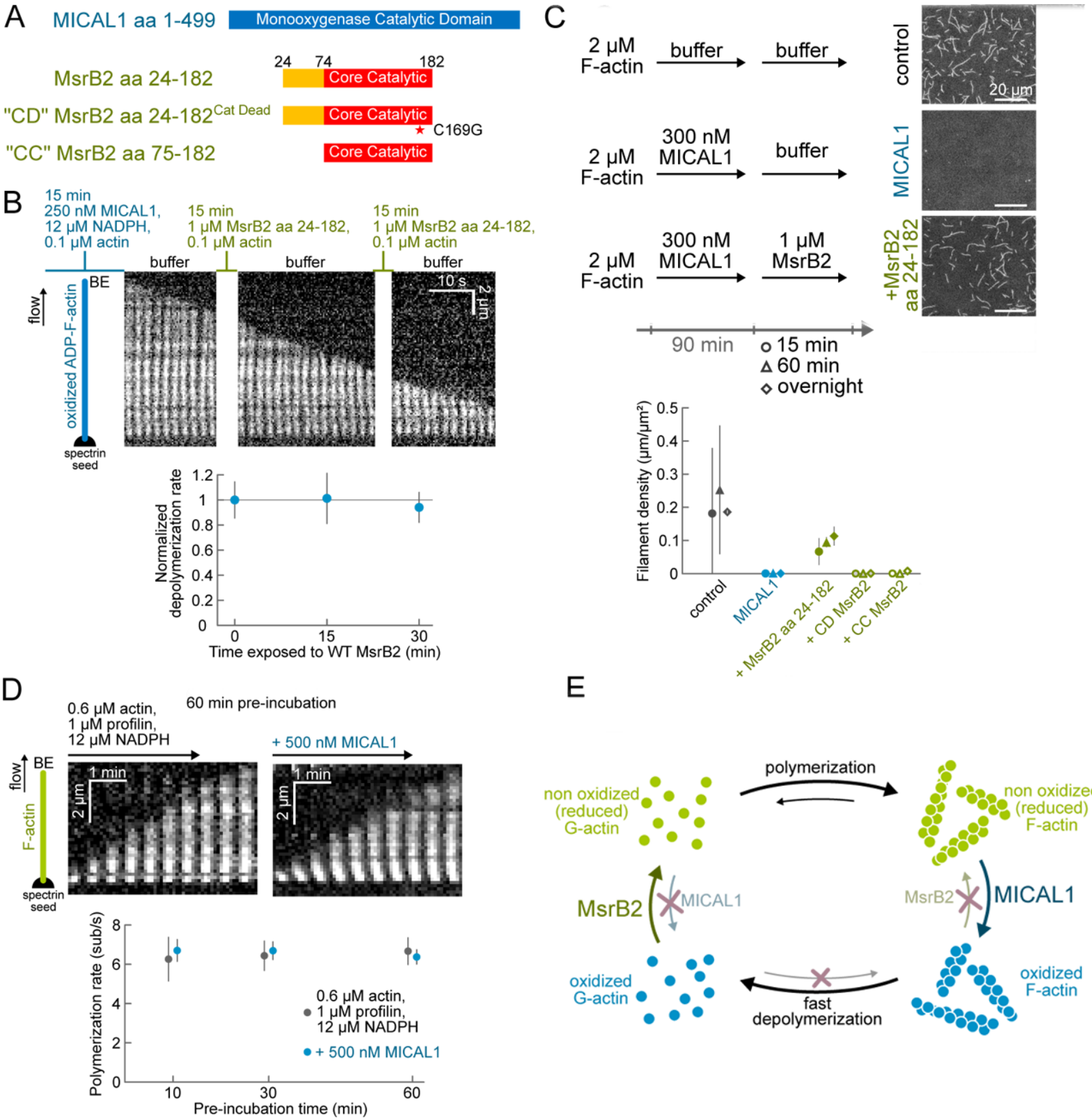
A
MICAL1 aa 1-499
Monooxygenase Catalytic Domain
MsrB2 aa 24-182
24
74
182
Core Catalytic
"CD" MsrB2 aa 24-182 Cat Dead
C169G
"CC" MsrB2 aa 75-182
B
15 min
250 nM MICAL1,
12 μM NADPH,
0.1 μM actin
15 min
1 μM MsrB2 aa 24-182,
0.1 μM actin
buffer
flow
BE
oxidized ADP-F-actin
spectrin seed
10 s
2 μm
Normalized depolymerization rate
Time exposed to WT MsrB2 (min)
C
2 μM F-actin
buffer
control
20 μm
300 nM MICAL1
MICAL1
1 μM MsrB2
+MsrB2 aa 24-182
90 min
15 min
60 min
overnight
Filament density (μm/μm²)
control
MICAL1
+ MsrB2 aa 24-182
+ CD MsrB2
+ CC MsrB2
D
0.6 μM actin,
1 μM profilin,
12 μM NADPH
60 min pre-incubation
+ 500 nM MICAL1
1 min
2 μm
F-actin
Polymerization rate (sub/s)
Pre-incubation time (min)
E
polymerization
non oxidized (reduced) G-actin
non oxidized (reduced) F-actin
MsrB2
MICAL1
oxidized G-actin
oxidized F-actin
fast depolymerization

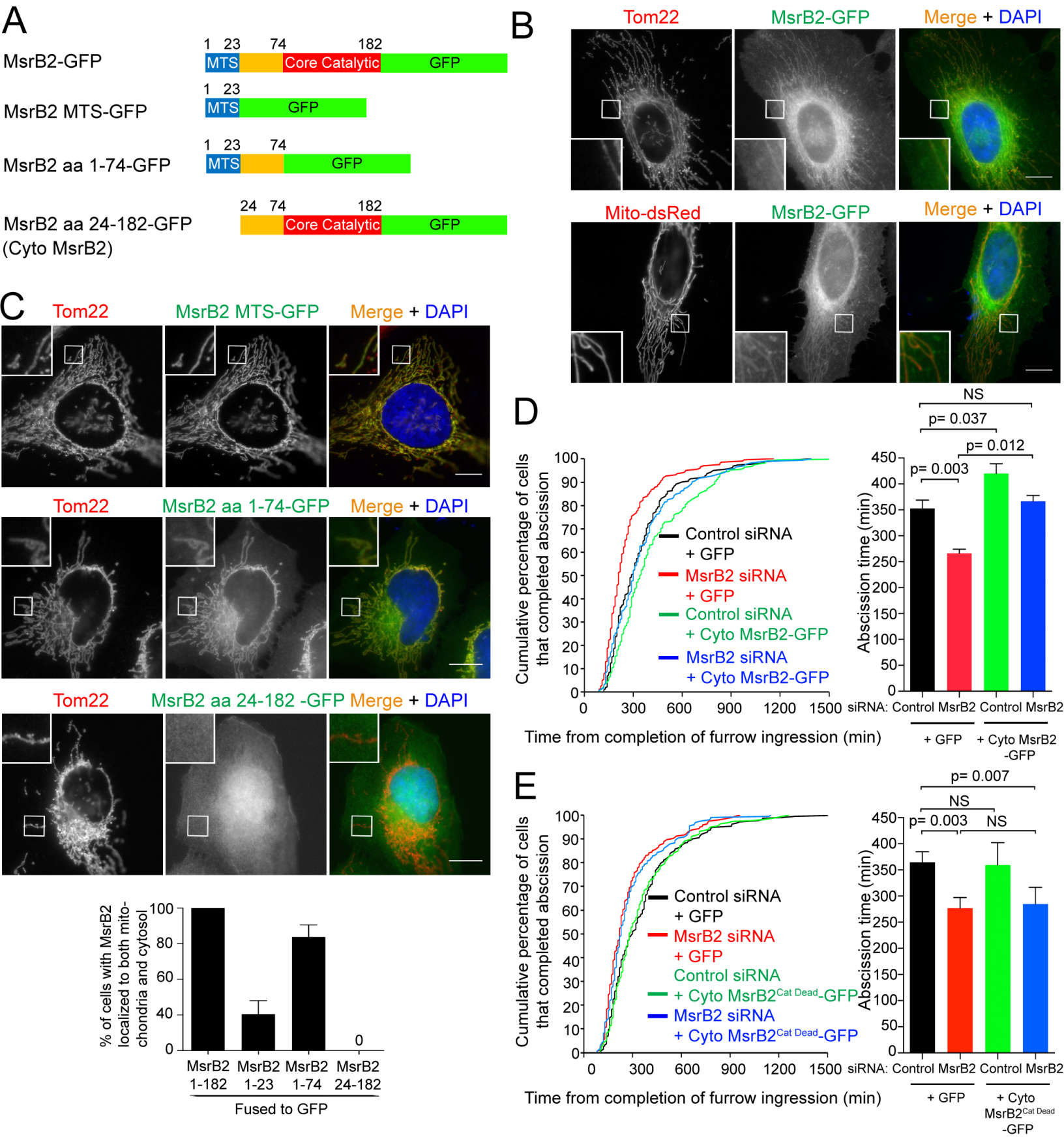
A
MsrB2-GFP
1 23 74 182
MTS
Core Catalytic
GFP
MsrB2 MTS-GFP
1 23
MTS
GFP
MsrB2 aa 1-74-GFP
1 23 74
MTS
GFP
MsrB2 aa 24-182-GFP
(Cyto MsrB2)
24 74 182
Core Catalytic
GFP
B
Tom22
MsrB2-GFP
Merge + DAPI
Mito-dsRed
MsrB2-GFP
Merge + DAPI
C
Tom22
MsrB2 MTS-GFP
Merge + DAPI
Tom22
MsrB2 aa 1-74-GFP
Merge + DAPI
Tom22
MsrB2 aa 24-182 -GFP
Merge + DAPI
% of cells with MsrB2 localized to both mitochondria and cytosol
MsrB2 1-182
MsrB2 1-23
MsrB2 1-74
MsrB2 24-182
Fused to GFP
D
Cumulative percentage of cells that completed abscission
Control siRNA + GFP
MsrB2 siRNA + GFP
Control siRNA + Cyto MsrB2-GFP
MsrB2 siRNA + Cyto MsrB2-GFP
Time from completion of furrow ingression (min)
NS
p= 0.037
p= 0.012
p= 0.003
Abscission time (min)
siRNA: Control MsrB2 Control MsrB2
+ GFP
+ Cyto MsrB2 -GFP
E
Cumulative percentage of cells that completed abscission
Control siRNA + GFP
MsrB2 siRNA + GFP
Control siRNA + Cyto MsrB2Cat Dead-GFP
MsrB2 siRNA + Cyto MsrB2Cat Dead-GFP
Time from completion of furrow ingression (min)
p= 0.007
NS
p= 0.003
NS
Abscission time (min)
siRNA: Control MsrB2 Control MsrB2
+ GFP
+ Cyto MsrB2Cat Dead -GFP

Figure 3

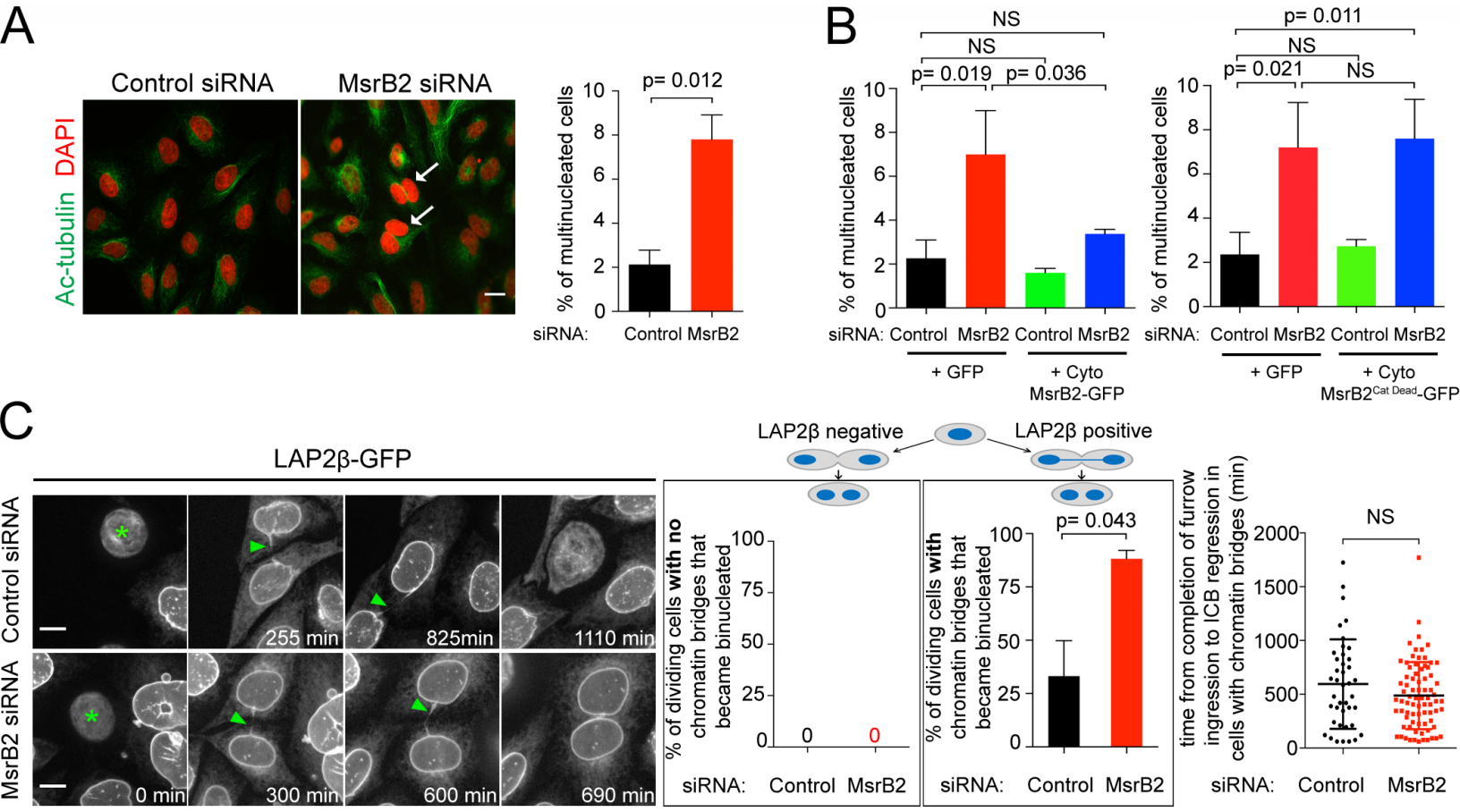
A
Control siRNA
MsrB2 siRNA
Ac-tubulin DAPI
p= 0.012
% of multinucleated cells
siRNA: Control MsrB2
B
NS
NS
p= 0.019 p= 0.036
% of multinucleated cells
siRNA: Control MsrB2 Control MsrB2
+ GFP
+ Cyto MsrB2-GFP
p= 0.011
NS
p= 0.021 NS
% of multinucleated cells
siRNA: Control MsrB2 Control MsrB2
+ GFP
+ Cyto MsrB2Cat Dead-GFP
C
LAP2β-GFP
Control siRNA
MsrB2 siRNA
255 min
825min
1110 min
0 min
300 min
600 min
690 min
LAP2β negative
LAP2β positive
% of dividing cells with no chromatin bridges that became binucleated
siRNA: Control MsrB2
p= 0.043
% of dividing cells with chromatin bridges that became binucleated
siRNA: Control MsrB2
NS
time from completion of furrow ingression to ICB regression in cells with chromatin bridges (min)
siRNA: Control MsrB2

Figure 4

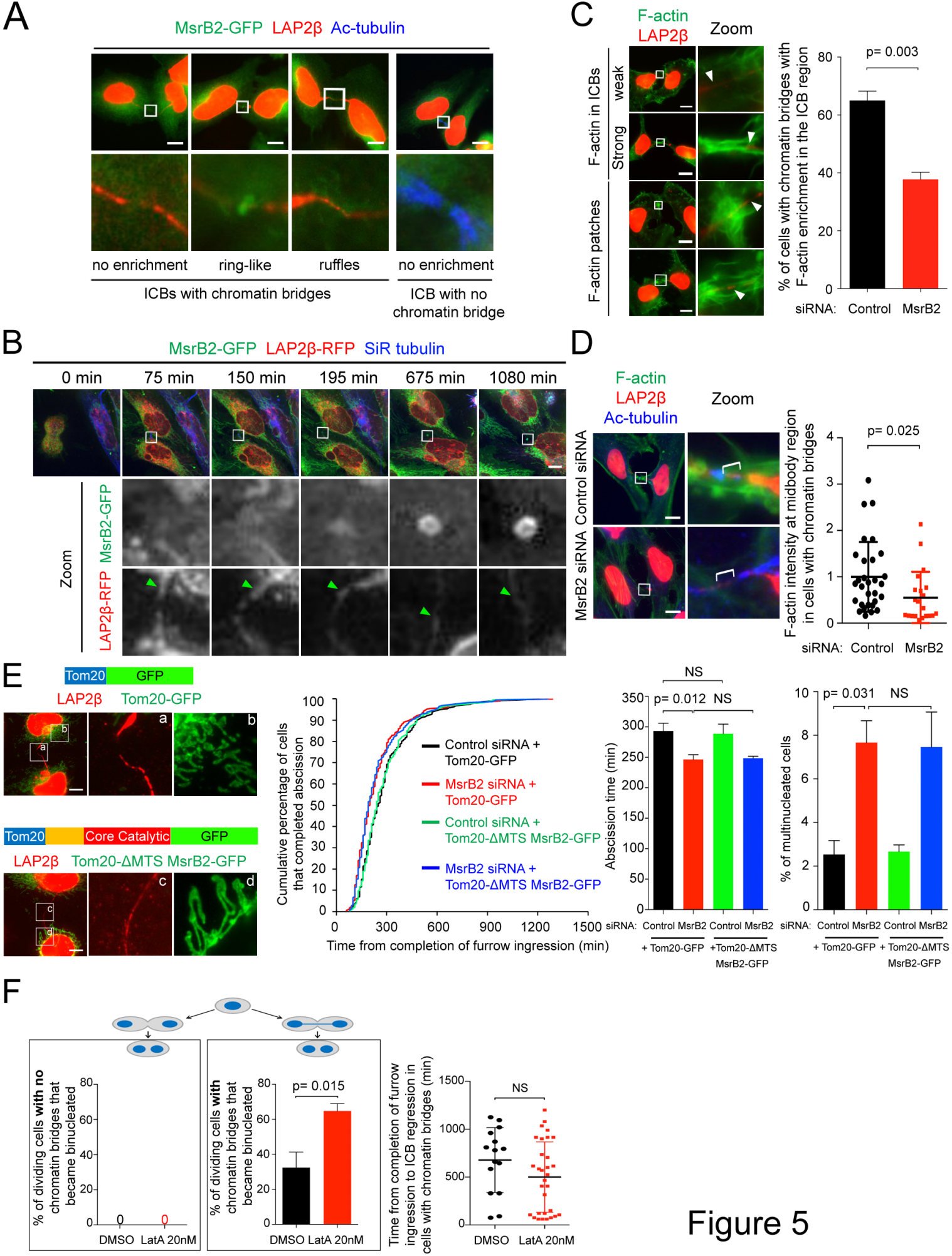
A
MsrB2-GFP LAP2β Ac-tubulin
no enrichment
ring-like
ruffles
no enrichment
ICBs with chromatin bridges
ICB with no chromatin bridge
B
MsrB2-GFP LAP2β-RFP SiR tubulin
0 min
75 min
150 min
195 min
675 min
1080 min
Zoom
MsrB2-GFP
LAP2β-RFP
C
F-actin
LAP2β
Zoom
F-actin in ICBs
weak
Strong
F-actin patches
% of cells with chromatin bridges with F-actin enrichment in the ICB region
p= 0.003
siRNA: Control MsrB2
D
F-actin
LAP2β
Ac-tubulin
Zoom
Control siRNA
MsrB2 siRNA
F-actin intensity at midbody region in cells with chromatin bridges
p= 0.025
siRNA: Control MsrB2
E
Tom20 GFP
LAP2β Tom20-GFP
Tom20 Core Catalytic GFP
LAP2β Tom20-ΔMTS MsrB2-GFP
Cumulative percentage of cells that completed abscission
Control siRNA + Tom20-GFP
MsrB2 siRNA + Tom20-GFP
Control siRNA + Tom20-ΔMTS MsrB2-GFP
MsrB2 siRNA + Tom20-ΔMTS MsrB2-GFP
Time from completion of furrow ingression (min)
Abscission time (min)
NS
p= 0.012
NS
siRNA: Control MsrB2 Control MsrB2
+ Tom20-GFP
+Tom20-ΔMTS MsrB2-GFP
% of multinucleated cells
p= 0.031
NS
siRNA: Control MsrB2 Control MsrB2
+ Tom20-GFP
+ Tom20-ΔMTS MsrB2-GFP
F
% of dividing cells with no chromatin bridges that became binucleated
DMSO LatA 20nM
% of dividing cells with chromatin bridges that became binucleated
p= 0.015
DMSO LatA 20nM
Time from completion of furrow ingression to ICB regression in cells with chromatin bridges (min)
NS
DMSO LatA 20nM

Figure 5

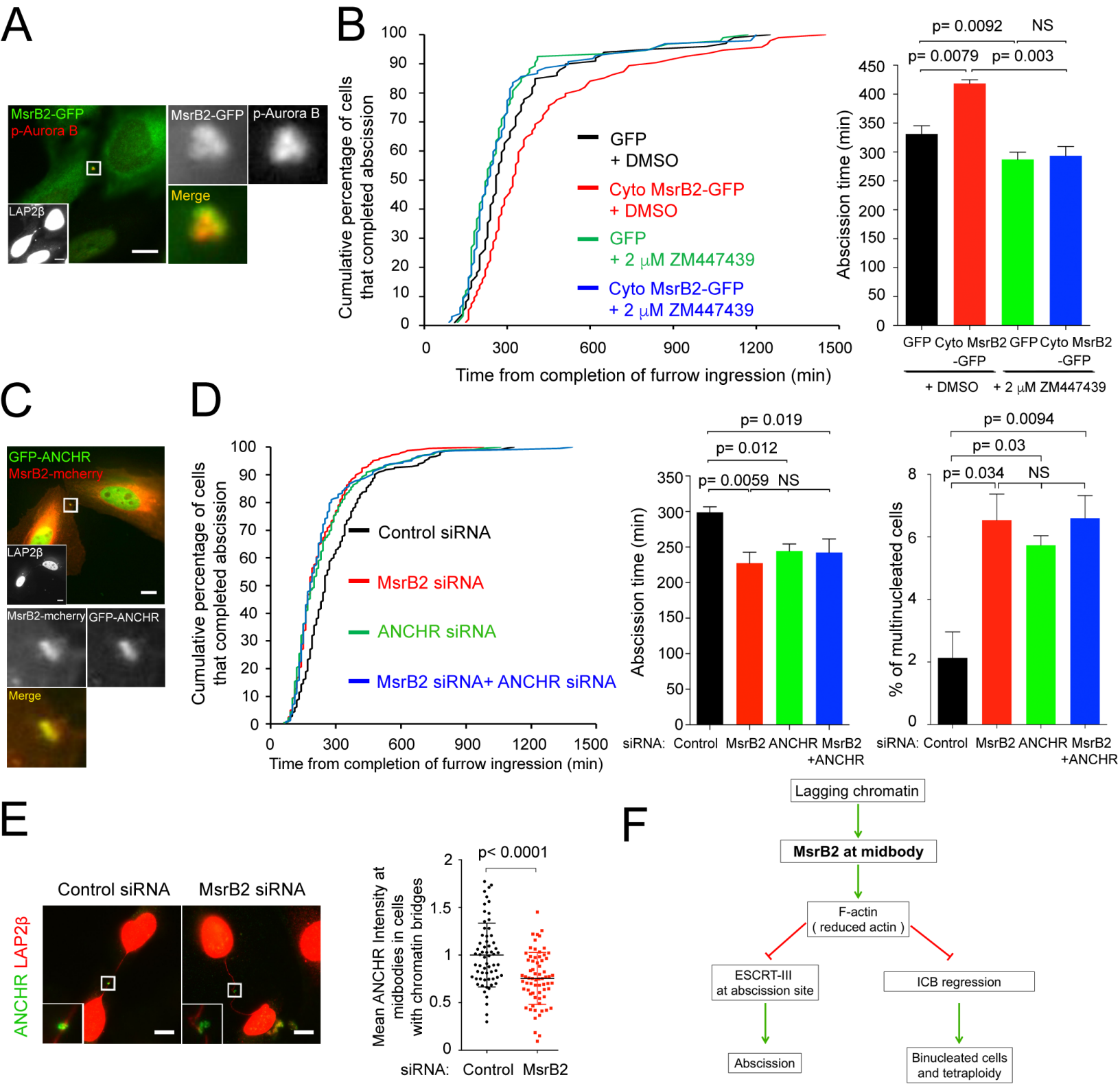
A
MsrB2-GFP
p-Aurora B
LAP2β
MsrB2-GFP
p-Aurora B
Merge
B
Cumulative percentage of cells that completed abscission
Time from completion of furrow ingression (min)
GFP + DMSO
Cyto MsrB2-GFP + DMSO
GFP + 2 μM ZM447439
Cyto MsrB2-GFP + 2 μM ZM447439
p= 0.0092
NS
p= 0.0079
p= 0.003
Abscission time (min)
GFP
Cyto MsrB2 -GFP
GFP
Cyto MsrB2 -GFP
+ DMSO
+ 2 μM ZM447439
C
GFP-ANCHR
MsrB2-mcherry
LAP2β
MsrB2-mcherry
GFP-ANCHR
Merge
D
Cumulative percentage of cells that completed abscission
Time from completion of furrow ingression (min)
Control siRNA
MsrB2 siRNA
ANCHR siRNA
MsrB2 siRNA+ ANCHR siRNA
p= 0.019
p= 0.012
p= 0.0059
NS
Abscission time (min)
siRNA: Control MsrB2 ANCHR MsrB2 +ANCHR
p= 0.0094
p= 0.03
p= 0.034
NS
% of multinucleated cells
siRNA: Control MsrB2 ANCHR MsrB2 +ANCHR
E
Control siRNA
MsrB2 siRNA
ANCHR LAP2β
p< 0.0001
Mean ANCHR Intensity at midbodies in cells with chromatin bridges
siRNA: Control MsrB2
F
Lagging chromatin
MsrB2 at midbody
F-actin (reduced actin)
ESCRT-III at abscission site
ICB regression
Abscission
Binucleated cells and tetraploidy

Figure 6

SI APPENDIX

Actin reduction by MsrB2 is a key component of the cytokinetic abscission checkpoint and prevents tetraploidy

Supplementary Methods and Information

Cell cultures

Drosophila Anillin-mCherry S2 cell line was generated and characterized in (1) (kind gift from Dr Gilles Hickson, St Justin, Montréal) and grown in Schneider medium (Invitrogen) at 26°C. HeLa cells cl2 from the ATCC were grown in Dulbecco's Modified Eagle Medium (DMEM) GlutaMax (31966; Gibco, Invitrogen Life Technologies) supplemented with 10% fetal bovine serum (FBS) and 1% Penicillin-Streptomycin (Gibco) in 5% CO2 condition at 37°C. HeLa LAP2β-GFP + H2B-RFP and Actin-GFP + LAP2β-RFP stable cell lines have been characterized in (2) (kind gifts from Dr Daniel Gerlich, IMBA, Vienna), and were cultured in DMEM with 10% FBS, 0.5 µg/ml puromycin and 0.5 mg/ml G418. For LatrunculinA experiments, Actin-GFP + LAP2β-RFP HeLa cells were treated with 20 nM LatrunculinA (Sigma-Aldrich).

Plasmids and siRNAs

Human *MsrB1, MsrB2* and *MsrB3B* cDNA were amplified by RT-PCR from HeLa cells, introduced into Gateway pENTR plasmid, then recombined into pGFP or pmCherry destination vector. MsrB2 truncated plasmids, including MsrB2 MTS-GFP, MsrB2 aa 1-74-GFP, MsrB2 aa 24-182-GFP were generated using the Gateway system, as for MsrB2-GFP. Point mutations (UGA into UGC at codon 95) in MsrB1 and C169G (Catalytically Dead, Cat Dead) in MsrB2-GFP and cyto MsrB2-GFP were generated using NEBaseChanger (NEB). SiRNA resistant versions of MsrB2-GFP, cyto MsrB2-GFP and their corresponding catalytically dead mutants have been obtained by mutating 6 bp of the siRNA-targeting sequence using NEBaseChanger (NEB). Tom20-GFP and Tom20-ΔMTS MsrB2-GFP plasmids were constructed by inserting the first 105 bp of Tom20 CDS to the 5' of GFP and siRNA-resistant MsrB2 aa 24-182-GFP, respectively, using NEBaseChanger (NEB). CRISPR guides targeting Luciferase (used as control, 5'-CGTACGCGGAATACTTCGA-3') and MsrB3 (5'-TGAGTGACATGGTACTGCAG-3') were cloned into PX330 plasmid (Addgene plasmid # 42230, from Dr. Feng Zhang) by using

the restriction enzyme BbsI. The LAP2β-RFP encoding plasmid was described in (2) (Addgene plasmid # 21047, from Dr. Daniel Gerlich). Mito-dsRed and GFP-ANCHR (3) encoding plasmids were a kind gifts from Dr.Tim Wai, Institut Pasteur, Paris and Dr. Harald Stenmark, University of Oslo, Norway, respectively.

RNAi in Drosophila S2 cells was carried out using the dSelR dsRNA targeting sequence amplified by PCR using the following primers: Forward: 5'TACTAATCGCACATCCAGAACG3', Reverse: 5'GTACTGTGTTGAATGTGTGGGG3' and transcribed in vitro, as described in (4). S2 cells were incubated with dsRNA for 3 days and movies were recorded for additional 2 days. Efficiency of RNAi was verified by western blot using dSelR antibody (see below). SiRNAs against Luciferase (used as control, 5'-CGUACGCGGAAUACUUCGA-3'), human MsrB2 (5'-GUUCUACGUCACAAGAGAA-3', (5)), human MICAL1 (5'-GAGUCCACGUCUCCGAUUU-3', (6)), human ANCHR (5'-GCACUAAUUCCAAGAGGCA-3') (3) and human Nup153 (5'-GGACUUGUUAGAUCUAGUU-3') (7) have been synthetized by Sigma-Aldrich. Human CEP55 (5'-UUCUUAAGGAGCUCCGAAA-3') siRNA was purchased from Dharmacon.

Antibodies

The following antibodies were used for western blot procedures: mouse anti-β-tubulin (1:5,000, Sigma-Aldrich T5168), rabbit anti-dSelR (1:1000, serum from immunized rabbits with recombinant dSelR isoform A (Uniprot: Q8INK9-2) AGRO-BIO, France), rabbit anti-MsrB2 (1:2000, serum from immunized rabbits with recombinant MsrB2 aa 24-182 by Covalab, France), rabbit anti-MICAL1 (1:500, Proteintech Europe 14818-1-AP), mouse anti-GAPDH (1:50000, Proteintech Europe 60004-1-Ig), rabbit anti-MsrB1 (1:300, Invitrogen LF-PA0088), rabbit anti-MsrB3 (1:1000, Abcam ab180584), mouse anti-CEP55 (1:1000, Santa Cruz Biotechnology 374051), rabbit anti-ANCHR (ref. 3, 1:1000, Bethyl Laboratories A301-808A), mouse anti-Nup153 (1:200, BioLegend MMS-102P). The following antibodies were used for immunofluorescence experiments: human anti-Acetylated-tubulin (PFA or methanol fixation, 1:500, C3B9-hFc, recombinant antibodies platform (TAb-IP) Curie antibodies platform (TAb-IP) Curie Institute, Paris, France), rabbit anti-CHMP4B (methanol fixation, 1:200, Santa Cruz Biotechnology 82557), mouse anti-TOM22 (PFA fixation, 1:1000, Sigma-Aldrich T6319), rabbit anti-pT232-Aurora B (PFA or methanol fixation, 1:200, Rockland) and mouse anti-LAP2β (PFA or methanol fixation, 1:500, BD biosciences), rabbit anti-ANCHR (methanol fixation, 1:4000, Bethyl Laboratories A301-808A). The following

secondary antibodies were used: Dylight Alexa 488- and Cy3- and Cy5-conjugated secondary antibodies (Jackson Laboratories) were diluted 1:500. Phalloidin conjugated with Alexa 488 (Invitrogen) was diluted 1:500.

Cell transfection

HeLa cells were transfected with plasmids for 24 h using X-tremeGENE 9 DNA reagent (Roche). For silencing experiments, HeLa cells were transfected twice with 50 nM siRNAs (MsrB2, MICAL1, ANCHR) or 20 nM siRNAs (for CEP55) for 96 h using HiPerFect (Qiagen) following the manufacturer's instructions. For Nup153 depletion experiments, cells were first treated with 50 nM MsrB2 siRNA for 24 h, then 50 nM MsrB2 siRNAs + 10 nM Nup153 siRNAs were transfected for an additional 72 h using HiPerFect (Qiagen) following the manufacturer's instructions. For the rescue experiments, cells were first transfected with siRNAs for 48 h using HiPerFect, then with plasmids using X-tremeGENE 9 DNA reagent for an additional 24 h. For CRISPR-Cas9 experiments, HeLa cells were transfected with 1 µg CRISPR plasmid and 200 ng of a puromycin resistant plasmid for 24 h using X-tremeGENE 9 DNA reagent. Cells were subsequently treated with 4 µg/ml puromycin overnight.

Western Blots

dsRNA-treated *Drosophila* S2 cells and siRNAs-treated HeLa cells were collected and lysed in 1x Laemmli (Bio-Rad Laboratories) with Benzonase nuclease. Lysates were migrated in 12% SDS-PAGE (Bio-Rad Laboratories), transferred onto PVDF membranes (Millipore) and incubated overnight with primary antibodies in 50 mM Tris-HCl pH 8.0, 150 mM NaCl, 0.1% Tween20, 5% milk followed by HRP-coupled secondary antibodies (1:10,000, Jackson Immuno Research) and revealed by chemiluminescence (GE Healthcare).

Immunofluorescence and image acquisition

HeLa cells were grown on coverslips and then fixed with the same volume of 8% paraformaldehyde (PFA) added to the culture medium for 10 min at room temperature and then replaced by 4% PFA for another 10 min, or fixed in pure methanol for 3 min at -20°C. Cells were permeabilized with 0.1% Triton X-100, blocked with PBS containing 1% BSA for 1 h at room temperature and successively incubated for 1 h at room temperature with primary and secondary antibody diluted in PBS containing 1% BSA (8). Cells were mounted in Mowiol

(Calbiochem). DAPI staining (0.5 mg/ml, Serva). Images were acquired with an inverted Ti E Nikon microscope, using a x 100 1.4 NA PL-APO objective lens or a × 40 1.4 NA PL-APO VC objective lens and MetaMorph software (MDS) driving a CCD camera (Photometrics Coolsnap HQ). Images were then converted into 8- bit images using ImageJ software (NIH).

To calculate the ratio mitochondria:cytosol of MsrB2-GFP for each cell quantified, an area of 60x60 pixels containing both cytosol and mitochondria was analyzed. Mitochondria location was determined by Tom22 staining and mean fluorescence intensity in the mitochondria or in the cytosol was measured using ImageJ software (NIH). Mean background intensity was subtracted from each measurement. The ratio of the mean intensity in the mitochondria to intensity in the cytosol is presented.

Time-lapse microscopy

For time-lapse phase-contrast microscopy, HeLa cells were seeded on 35 mm glass dishes or glass bottom 12-well plates (MatTek) and put in an open chamber (Life Imaging) equilibrated in 5% CO2 and maintained at 37 °C. Time-lapse sequences were recorded at 10 min intervals for 48 h using a Nikon Eclipse Ti inverted microscope with a ×20 0.45 NA Plan Fluor ELWD objective lens controlled by Metamorph software (MDS). For time-lapse fluorescent spinning disk confocal microscopy, time-lapse sequences were recorded at 15 min intervals for 36 h or 48 h using an inverted Eclipse TiE Nikon microscope equipped with a CSU-X1 spinning disk confocal scanning unit (Yokogawa) and with a EMCCD Camera (Evolve 512 Delta, Photometrics). Images were acquired with a x40 or a x60 1.4 NA PL-APO VC and MetaMorph software (MDS).

Time-lapse phase-contrast microscopy after Aurora B inhibition was carried out as previously described (2, 9), using HeLa cells transfected with either GFP or cyto MsrB2-GFP. The day after, 50 000 cells were plated in glass bottom 12-well plates (MaTtek). The following day, positions containing green fluorescent round, mitotic cells were recorded for 24 h every 10 min in phase contrast, using an inverted Eclipse TiE Nikon microscope equipped with a CSU-X1 spinning disk confocal scanning unit (Yokogawa) and with a EMCCD Camera (Evolve 512 Delta, Photometrics). Images were acquired with a ×20 0.45 NA Plan Fluor ELWD objective lens controlled by Metamorph software (MDS). DMSO or 2μM ZM447439 (Aurora B inhibitor, Sigma-Aldrich) were added to the wells between time points 80 min and 90 min, thus after completion of furrow ingression.

Protein purification

The full-length coding sequence of d*SelR* isoform A was amplified by RT-PCR from *Drosophila* S2 cells, introduced into Gateway pENTR plasmid and recombined with 6xHis tagged destination vector. 6xHis-tagged dSelR was expressed in the *Escherichia coli* BL21-DE3 pLysS strain after induction with 1 mM isopropyl-β-D-thiogalactopyranoside at 18 °C for 24 h. Recombinant dSelR protein was affinity-purified using Ni-NTA Magnetic Agarose Beads (Qiagen), eluted in 50 mM Tris pH 8, 150 mM NaCl, 2 mM MgCl2 and 250 mM Imidazole and dialyzed at 4°C overnight in 50 mM Tris pH 8, 150 mM NaCl, 1 mM DTT. Purified 6xHis-tagged dSelR protein was used for rabbit immunization to generate anti-dSelR antibodies.

For *in vitro* actin polymerization/depolymerization experiments (Fig. 2), plasmids encoding GST-TEV-cyto MsrB2 (aa 24-182), GST-TEV-cyto MsrB2$^{Cat\ Dead}$ (aa 24-182 with C169G) and GST-TEV-MsrB2 core catalytic domain (aa 75-182) were constructed by inserting the corresponding cDNAs into pGST//2 vector containing a TEV protease recognition site upstream to MsrB2s, using the restriction enzymes NcoI and EcoRI. The three corresponding proteins were expressed in *Escherichia coli* BL21-DE3 pLysS strain after induction with 1 mM isopropyl-β-D-thiogalactopyranoside at 18 °C for 24 h and were affinity-purified in parallel using glutathione Sepharose 4B (GE Healthcare), eluted by incubating the beads with 10 µg/ml of TEV protease (Recombinant antibodies platform (TAb-IP) Curie Institute, Paris, France) in PBS at 30°C for 2 h. The purified cyto MsrB2 protein was also used for rabbit immunization to generate anti-MsrB2 antibodies.

The catalytic domain of human MICAL1 was purified as described in (6).

Alpha-skeletal muscle actin was purified from home-made rabbit muscle acetone powder, following the protocol described in (10), adapted from the original protocol (11). Spectrin-actin seeds were purified from human erythrocytes as described in (10), based on the original protocol (12). Recombinant human profilin I (Uniprot : P07737) was expressed in *E. coli* and purified following the protocol described in (13).

Actin was fluorescently labeled on accessible surface lysines of F-actin, using Alexa-488 succinimidyl ester (Life Technologies).

Buffers for *in vitro* experiments (Fig. 2)

In vitro experiments were performed in F-buffer: 5 mM Tris HCl pH 7.8, 50 mM KCl, 1 mM MgCl2, 0.2 mM EGTA, 0.2 mM ATP, 10 mM DTT and 1 mM DABCO (DTT and DABCO limit light-induced artifacts).

Measurements of actin polymerization and depolymerization rates (Fig. 2B, D)

Experiments were performed inside a microfluidic chamber following a standard procedure (10, 14). Briefly, the microfluidic chamber consisted of a PDMS block and a cleaned glass coverslip, treated with UV and bound together. The chamber was 20 µm in height. It contained 3 to 4 inlets and one outlet, connected to protein solutions through a pressure-controlling device and flow meters (Fluigent).

The glass surface was first functionalized with spectrin-actin seeds (30 pM, 2 min) and passivated with BSA (5%, 10 min). Filaments were polymerized by injecting a solution of ATP-G-actin (10% labeled on lysines with Alexa-488), profilin (to prevent spontaneous nucleation in solution) and sometimes NADPH and MICAL1.

Prior to looking at depolymerization, filaments were aged with a solution of G-actin at the critical concentration (0.1 µM, 15 min), in order to ensure complete (>99%) ATP hydrolysis and Pi release. MICAL1 and NADPH were sometimes included in this solution, to oxidize filaments. Depolymerization was then triggered by exposing filaments to buffer only.

Acquisition: Movies were acquired on an inverted microscope (Nikon Eclipse Ti, 60x objective), under TIRF or epifluorescence illumination (Ilas2, Gataca Systems), using an Evolve EMCCD camera (Photometrics).

Analysis: Movies were analyzed in ImageJ. Polymerization and depolymerization rates were measured manually on kymographs.

G-actin reduced by MsrB2 (Fig. 2C)

Biochemical reactions were performed in bulk solutions. F-buffer was supplemented with 12 µM NADPH and 5 mM DTT. 6 µM actin were first polymerized in this buffer (>1h) before adding 300 nM MICAL1 (90 min), yielding a solution of oxidized G-actin (in the control experiment, buffer was added instead of MICAL1, yielding a solution of non-oxidized F-actin). Buffer or 1 µM MsrB2 was next added to the solution. After 15 min, 60 min or overnight, a fraction of the solution was diluted 20-fold into F-buffer supplemented with

0.3% methylcellulose and injected into a BSA-passivated open chamber, made of two glass coverslips separated by double-sided tape. Filaments were visualized a couple of minutes after injection.

Acquisition: Movies were acquired on an inverted microscope (Nikon Eclipse Ti, 60x objective), with epifluorescence illumination (Lumen Dynamics), using a sCMOS Orca-Flash2.8 camera (Hamamatsu).

Analysis: when the actin filament density was significant (conditions Control and +WT MsrB2), it was quantified by measuring the total fluorescence signal (minus background) normalized by the fluorescence of a filament of known length. When the actin filament density was extremely low (conditions MICAL1, +CC MsrB2, +CD MsrB2), this method would estimate densities to be compatible with zero, so instead we manually measured the total length of filaments in order to be more accurate.

Statistical analysis.

All values are displayed as mean ± SDs for three independent experiments (as indicated in the figure legends). Significance was calculated using Student t-tests, as indicated. For accumulative graph of abscission times, a non-parametric Kolmogorov–Smirnov test was used.

Supplementary References

1. El Amine N, Kechad A, Jananji S, & Hickson GR (2013) Opposing actions of septins and Sticky on Anillin promote the transition from contractile to midbody ring. *The Journal of cell biology* 203(3):487-504.
2. Steigemann P*, et al.* (2009) Aurora B-mediated abscission checkpoint protects against tetraploidization. *Cell* 136(3):473-484.
3. Thoresen SB*, et al.* (2014) ANCHR mediates Aurora-B-dependent abscission checkpoint control through retention of VPS4. *Nature cell biology*.
4. Echard A, Hickson GR, Foley E, & O'Farrell PH (2004) Terminal Cytokinesis Events Uncovered after an RNAi Screen. *Current biology : CB* 14(18):1685-1693.
5. Marchetti MA*, et al.* (2005) Methionine sulfoxide reductases B1, B2, and B3 are present in the human lens and confer oxidative stress resistance to lens cells. *Invest Ophthalmol Vis Sci* 46(6):2107-2112.
6. Fremont S*, et al.* (2017) Oxidation of F-actin controls the terminal steps of cytokinesis. *Nat Commun* 8:14528.

7. Mackay DR, Makise M, & Ullman KS (2010) Defects in nuclear pore assembly lead to activation of an Aurora B-mediated abscission checkpoint. *The Journal of cell biology* 191(5):923-931.
8. Crowell EF, Gaffuri AL, Gayraud-Morel B, Tajbakhsh S, & Echard A (2014) Midbody remnant engulfment after cytokinesis abscission in mammalian cells. *J Cell Sci* 127(17):3840-3851.
9. Mathieu J*, et al.* (2013) Aurora B and cyclin B have opposite effects on the timing of cytokinesis abscission in Drosophila germ cells and in vertebrate somatic cells. *Developmental cell* 26(3):250-265.
10. Wioland H*, et al.* (2017) ADF/Cofilin Accelerates Actin Dynamics by Severing Filaments and Promoting Their Depolymerization at Both Ends. *Current biology : CB* 27(13):1956-1967 e1957.
11. Spudich JA & Watt S (1971) The regulation of rabbit skeletal muscle contraction. I. Biochemical studies of the interaction of the tropomyosin-troponin complex with actin and the proteolytic fragments of myosin. *The Journal of biological chemistry* 246(15):4866-4871.
12. Casella JF, Maack DJ, & Lin S (1986) Purification and initial characterization of a protein from skeletal muscle that caps the barbed ends of actin filaments. *The Journal of biological chemistry* 261(23):10915-10921.
13. Gieselmann R, Kwiatkowski DJ, Janmey PA, & Witke W (1995) Distinct biochemical characteristics of the two human profilin isoforms. *Eur J Biochem* 229(3):621-628.
14. Jegou A*, et al.* (2011) Individual actin filaments in a microfluidic flow reveal the mechanism of ATP hydrolysis and give insight into the properties of profilin. *PLoS biology* 9(9):e1001161.
15. Kim HY & Gladyshev VN (2004) Methionine sulfoxide reduction in mammals: characterization of methionine-R-sulfoxide reductases. *Molecular biology of the cell* 15(3):1055-1064.

Supplementary Figure legends

Figure S1: dSelR and MsrB2 are negative regulators of cytokinetic abscission in cultured cells.

(A) Left: lysates from *Drosophila* S2 control cells and dSelR dsRNA treated cells were blotted for dSelR and α-tubulin (loading control). Middle and Right: distribution of the abscission time ($p< 0.001$, KS test) and mean abscission time ± SD in control and dSelR-depleted cells ($N=3$). n=257-279 cells per condition. NS, not significant. p value (Student-t test) is indicated.

(*B*) Snapshot of time-lapse phase-contrast microscopy movies of HeLa cells depleted with control or MsrB2 siRNA. Red arrows mark the midbody. Scale bar: 10 µm.

(C) Left: lysates from the same cell populations used in the Figure 1B left panel were blotted for MsrB2 and GAPDH (loading control). Right: lysates from the same cell populations used in the Figure 1B middle panel were blotted for MsrB2 and GAPDH (loading control).

Figure S2: MsrB1 and MsrB3 do not play role in cytokinesis.

(A) Left: lysates from Control and MsrB3 CRISPR-Cas9-treated cells were blotted for MsrB3 and GAPDH (loading control). Middle and Right: distribution of the abscission time ($p= 0.715$,

KS test) and abscission time for Control and MsrB3 CRISPR-Cas9-treated cells. Mean ± SD (N=3). n=244-248 cells per condition.

(B) Upper left panel: lysates from control or MsrB2 siRNA-treated cells and transfected with indicated plasmids were blotted for MsrB1 (intermediate blot), MsrB2 (lower blot), MsrB3 (upper blot) or GAPDH (loading control, intermediate blot). Endogenous MsrB1 was not detected. Upper middle panel: representative image of a cell transfected with MsrB1^{U95C}-GFP (green) and stained with DAPI (blue). MsrB1 is a selenocysteine containing protein and the MsrB1^{U95C} has a cysteine instead of a selenocysteine, but retains catalytic activity (15). Upper right panel: representative image of a cell transfected with MsrB3B-GFP (green) and stained with DAPI (blue). Note that both MsrB1^{U95C}-GFP and MsrB3B-GFP were cytosolic (zooms). Intermediate panels: distribution of the abscission time (left) and mean abscission time ± SD (right) for control- and MsrB2-depleted cells transfected with indicated plasmids (*N=3*). No statistical difference between black and green curves, or between red and blue curves. *p*< 0.001 between black and red curves (KS tests). n=222-229 cells per condition. Bottom panels: distribution of the abscission time (left) and mean abscission time ± SD (right) for control- and MsrB2-depleted cells transfected with indicated plasmids (*N=3*). No statistical difference between black and green curves, or between red and blue curves. *p*< 0.001 between black and red curves (KS tests). n=213-216 cells per condition. NS, not significant. p values (Student-t tests) are indicated.

Figure S3: MsrB2 depletion does not destabilize ICBs of cells arrested in cytokinesis after CEP55 depletion.

(A) The ratio of the mean fluorescence intensity in the mitochondria and in the cytosol in cells transiently transfected with MsrB2$^{1-182}$-GFP, MsrB2$^{1-23}$-GFP, MsrB2$^{1-74}$-GFP or MsrB2$^{24-182}$ is provided. As a control, the ratio mitochondria:cytosol was measured for GFP alone (localized in the cytoplasm) or Tom20$^{1-35}$GFP (localized at the mitochondria). n=30 cells per condition. Mean ± SD.

(B) Left: lysates from the same cell populations used in Figure 3D were blotted for MsrB2 and GAPDH (loading control). Right: lysates from the same cell populations used in Figure 3E were blotted for MsrB2 and GAPDH (loading control).

(C) Left: lysates from cells treated with either control, MsrB2, CEP55 or MsrB2+CEP55 siRNAs were blotted for CEP55, MsrB2 and GAPDH (loading control). Middle: percentage of

cells connected by tubulin-positive ICBs (*N=3*). Note that one ICB was counted for two connected cells, thus 50% of the cells were at cytokinesis upon CEP55 depletion. n= 1500 cells per condition. Mean ± SD. Right: percentage of multinucleated cells after control, MsrB2, CEP55 and MsrB2+CEP55 depletion (*N*=3). n=1500 cells per condition. Mean ± SD. p values (Student-t tests) are indicated.

Figure S4: MsrB2 is required for delaying abscission upon checkpoint activation by nuclear pore defects.

(A) Snapshot of a time-lapse spinning disk confocal microscopy movie of cells expressing MsrB2-GFP (green) and LAP2β-RFP (red), labeled with SiR-tubulin (blue). Brackets mark the midbody. Scale bar: 10 µm.

(*B*) Mean F-actin intensity (fluorescent phalloidin) in the cell bodies of cells treated with either control, MsrB2, MICAL1 or MsrB2+MICAL1 siRNAs (*N=3*). n=32-54 cells per condition. Mean ± SD are indicated.

(C) Lysates from the same cell populations used in Figure 5E were blotted for MsrB2 and GAPDH (loading control).

(*D*) Left: representative images of control- and MsrB2-depleted cells stained with pT232 Aurora B (green) and LAP2β (red). Scale bar: 10 µm. Right: quantification of pT232 Aurora B intensity at the midbody (arbitrary units) in control- and MsrB2-depleted cells with chromatin bridges (*N=3*). n=64-67 cells per condition.

(*E*) Lysates from the same cell populations used in Figure 6D were blotted for ANCHR, MsrB2 and GAPDH (loading control).

(F) Left: lysates from cells treated with either control, MsrB2, Nup153 or MsrB2+Nup153 siRNAs were blotted with Nup153, MsrB2 and GAPDH (loading control). Middle and Right: distribution of abscission time and mean abscission time ± SD for the same cell populations used in left panel (*N=3*). n=234-262 cells per condition. For comparisons between distributions (KS tests): p= 0.01 between black and blue curves; p< 0.001 for all other comparisons. For comparisons between means: NS, not significant. p values (Student-t tests) are indicated.

Supplementary Movie Legends

Movie S1: Abscission is delayed but no binucleated cells are formed in a control-depleted cell with a chromatin bridge.

Live cells stably expressing LAP2β-GFP were treated with control siRNAs and recorded with spinning disk confocal microscopy and a 40x objective every 15 min for 48 h. Time indicated in hr:min. Scale bar: 5 µm.

Movie S2: MsrB2 depletion results in ICB regression and binucleation in a cell with a chromatin bridge.

Live cells stably expressing LAP2β-GFP were treated with MsrB2 siRNAs and recorded with a spinning disk confocal microscopy and a 40x objective every 15 min for 48 h. Time indicated in hr:min. Scale bar: 5 µm.

Movie S3: MsrB2-GFP localization during cytokinesis in a dividing cell without a chromatin bridge.

Live cells expressing MsrB2-GFP (green) and LAP2β-RFP (red) were labeled with SiR-tubulin (blue) and recorded with a spinning disk confocal microscopy and a 60x objective every 15 min for 48 h. Time indicated in hr:min. Scale bar: 10 µm.

Movie S4: MsrB2-GFP localization during cytokinesis in a dividing cell with a chromatin bridge.

Live cells expressing MsrB2-GFP (green) and LAP2β-RFP (red), was labeled with SiR-tubulin (blue) and recorded with a spinning disk confocal microscopy and a 60x objective every 15 min for 48 h. Time indicated in hr:min. Scale bar: 10 µm.

Movie S5: Abscission is delayed but no binucleated cells are formed in a control (DMSO)-treated cell with a chromatin bridge.

Live cells stably expressing LAP2β-RFP were treated with 0.05% DMSO (control) and recorded with a spinning disk confocal microscopy and a 60x objective every 15 min for 36 h. Time indicated in hr:min. Scale bar: 10 µm.

Movie S6: Treatment with 20 nM of LatrunculinA in a cell with a chromatin bridge results in the regression of the ICB and binucleation.

Live cells stably expressing LAP2β-RFP were treated with 20 nM LatrunculinA and recorded with a spinning disk confocal microscopy and a 60x objective every 15 min for 36 h. Scale bar: 10 µm.

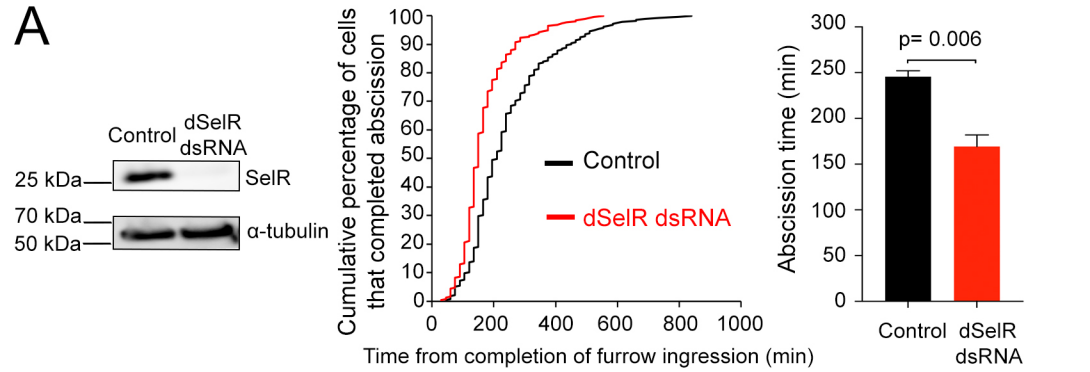
A
Control
dSelR dsRNA
25 kDa
SelR
70 kDa
50 kDa
α-tubulin
Cumulative percentage of cells that completed abscission
Control
dSelR dsRNA
Time from completion of furrow ingression (min)
Abscission time (min)
p= 0.006
Control
dSelR dsRNA

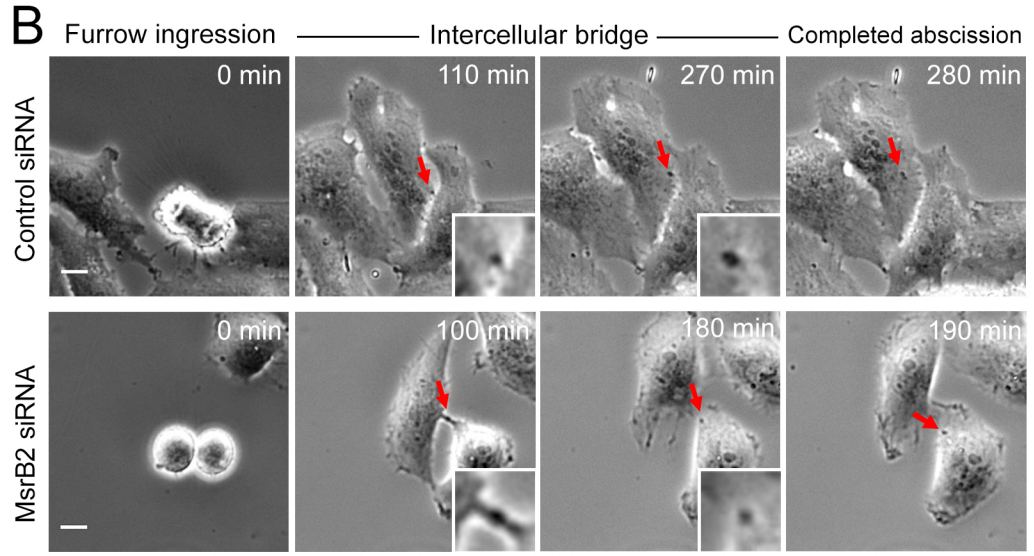
B
Furrow ingression
Intercellular bridge
Completed abscission
Control siRNA
0 min
110 min
270 min
280 min
MsrB2 siRNA
0 min
100 min
180 min
190 min

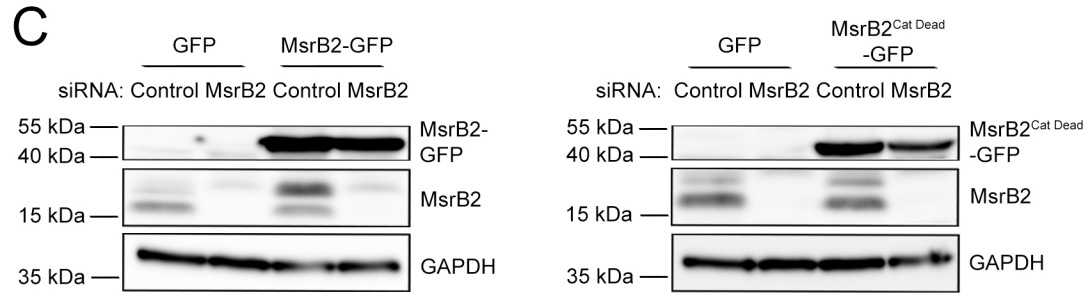
C
GFP
MsrB2-GFP
siRNA: Control MsrB2 Control MsrB2
55 kDa
40 kDa
MsrB2-GFP
15 kDa
MsrB2
35 kDa
GAPDH
GFP
MsrB2Cat Dead -GFP
siRNA: Control MsrB2 Control MsrB2
55 kDa
40 kDa
MsrB2Cat Dead -GFP
15 kDa
MsrB2
35 kDa
GAPDH

Figure S1

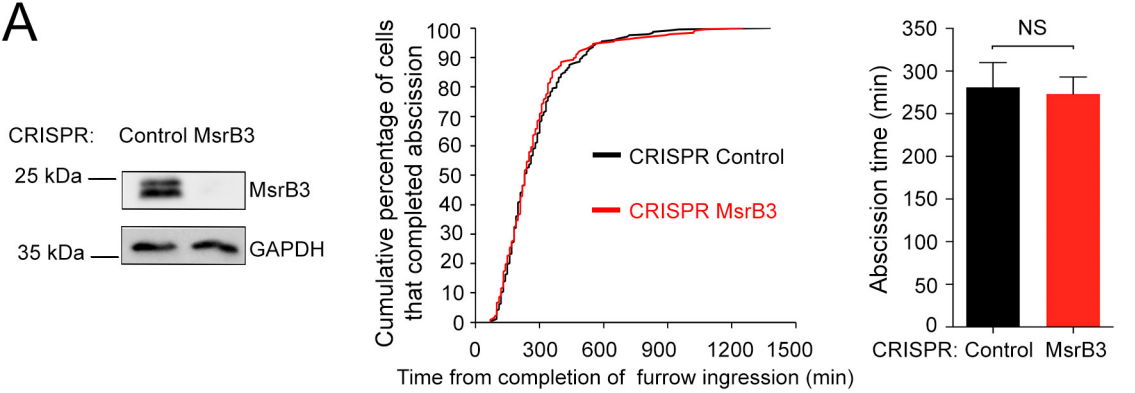
A
CRISPR: Control MsrB3
25 kDa
MsrB3
35 kDa
GAPDH
Cumulative percentage of cells that completed abscission
Time from completion of furrow ingression (min)
CRISPR Control
CRISPR MsrB3
Abscission time (min)
NS
CRISPR: Control MsrB3

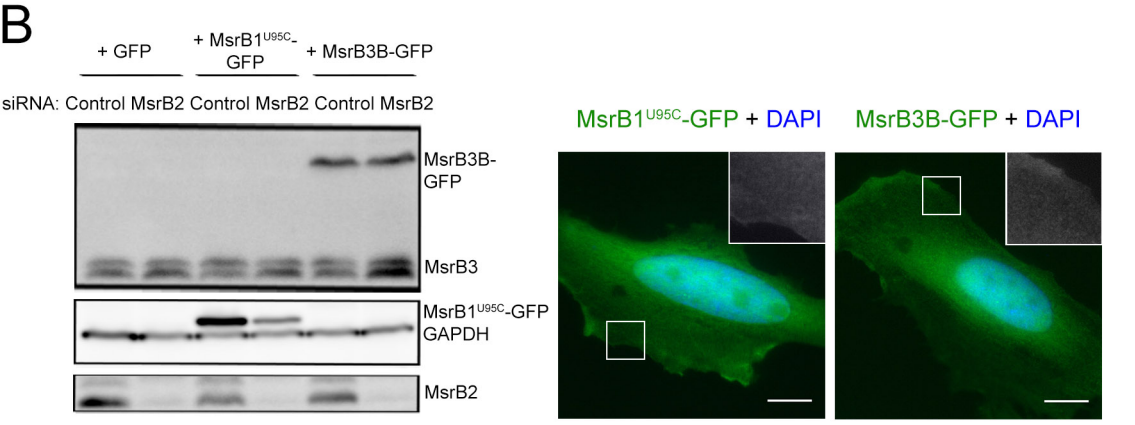
B
+ GFP
+ MsrB1U95C-GFP
+ MsrB3B-GFP
siRNA: Control MsrB2 Control MsrB2 Control MsrB2
MsrB3B-GFP
MsrB3
MsrB1U95C-GFP
GAPDH
MsrB2
MsrB1U95C-GFP + DAPI
MsrB3B-GFP + DAPI

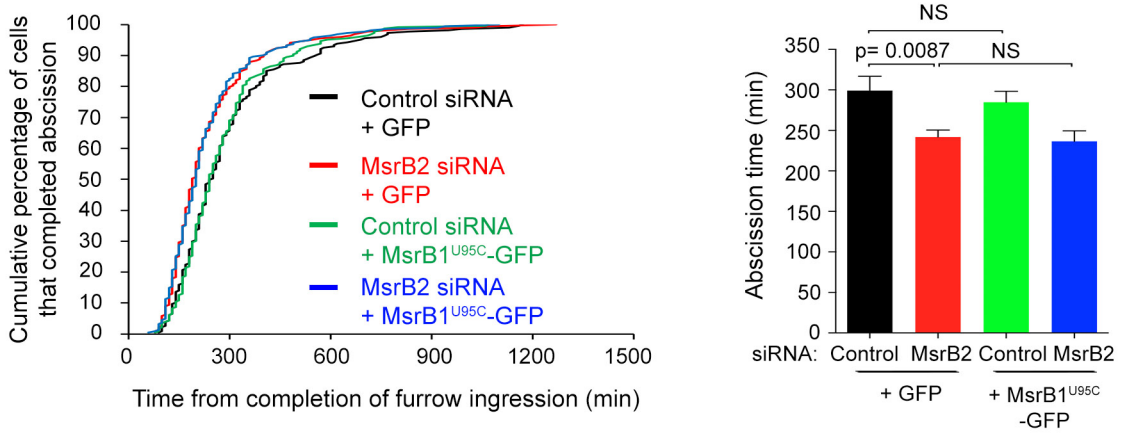
Cumulative percentage of cells that completed abscission
Time from completion of furrow ingression (min)
Control siRNA + GFP
MsrB2 siRNA + GFP
Control siRNA + MsrB1U95C-GFP
MsrB2 siRNA + MsrB1U95C-GFP
Abscission time (min)
NS
p= 0.0087
NS
siRNA: Control MsrB2 Control MsrB2
+ GFP
+ MsrB1U95C -GFP

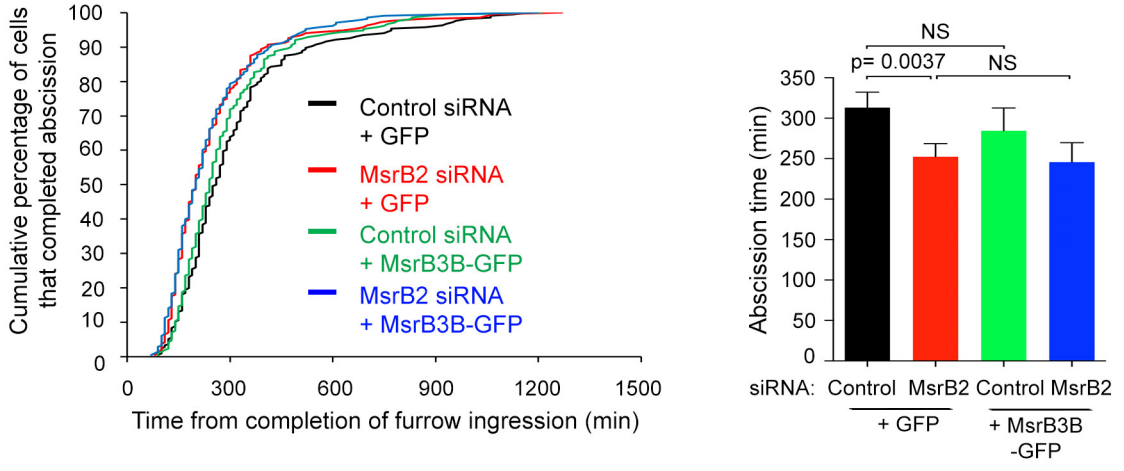
Cumulative percentage of cells that completed abscission
Time from completion of furrow ingression (min)
Control siRNA + GFP
MsrB2 siRNA + GFP
Control siRNA + MsrB3B-GFP
MsrB2 siRNA + MsrB3B-GFP
Abscission time (min)
NS
p= 0.0037
NS
siRNA: Control MsrB2 Control MsrB2
+ GFP
+ MsrB3B -GFP

Figure S2

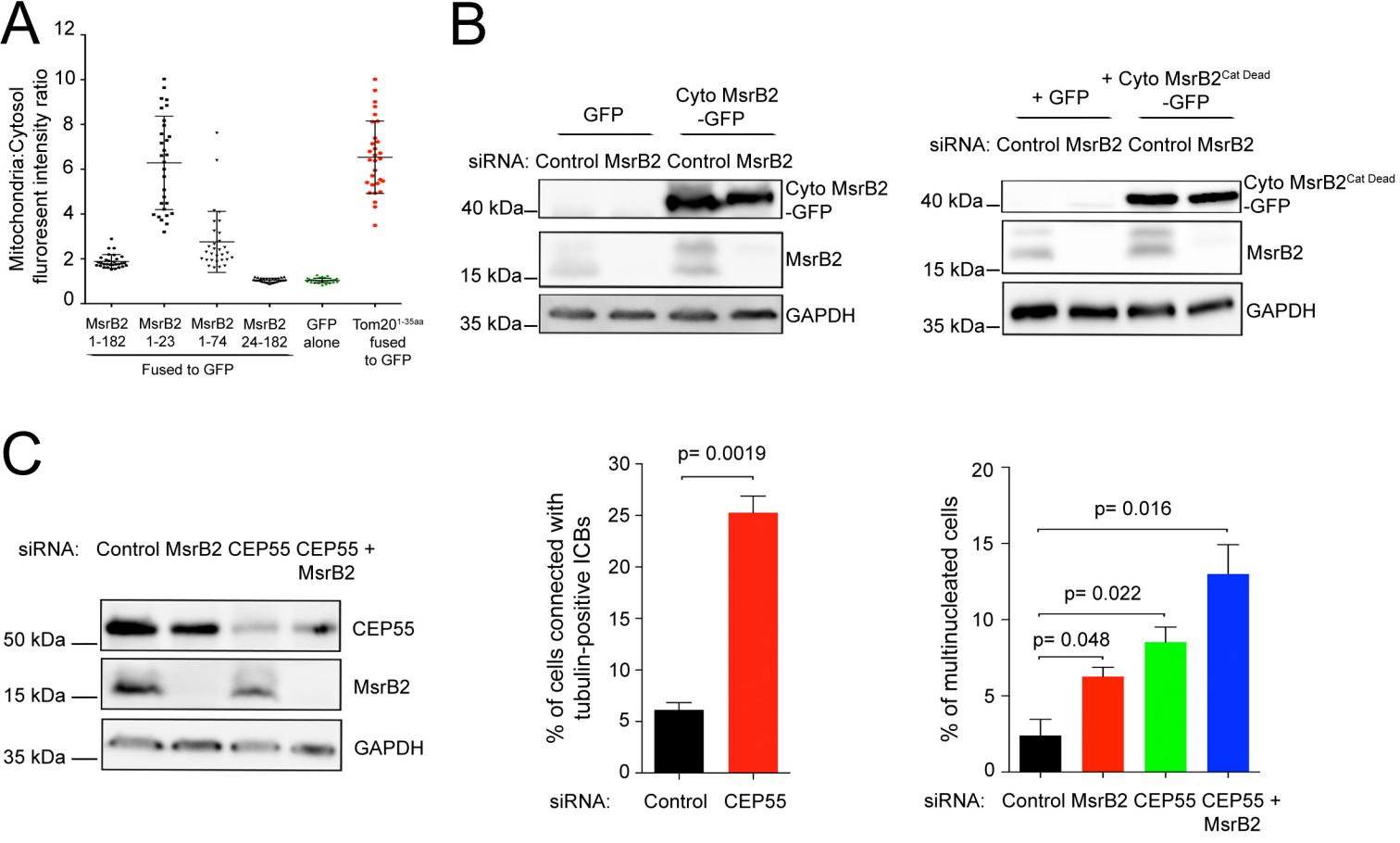
A
Mitochondria:Cytosol fluorescent intensity ratio
12
10
8
6
4
2
0
MsrB2 1-182
MsrB2 1-23
MsrB2 1-74
MsrB2 24-182
GFP alone
Tom20 1-35aa fused to GFP
Fused to GFP
B
GFP
Cyto MsrB2 -GFP
siRNA: Control MsrB2 Control MsrB2
40 kDa
15 kDa
35 kDa
Cyto MsrB2 -GFP
MsrB2
GAPDH
+ GFP
+ Cyto MsrB2Cat Dead -GFP
siRNA: Control MsrB2 Control MsrB2
40 kDa
15 kDa
35 kDa
Cyto MsrB2Cat Dead -GFP
MsrB2
GAPDH
C
siRNA: Control MsrB2 CEP55 CEP55 + MsrB2
50 kDa
15 kDa
35 kDa
CEP55
MsrB2
GAPDH
% of cells connected with tubulin-positive ICBs
p= 0.0019
30
25
20
15
10
5
0
siRNA: Control CEP55
% of multinucleated cells
p= 0.016
p= 0.022
p= 0.048
20
15
10
5
0
siRNA: Control MsrB2 CEP55 CEP55 + MsrB2

Figure S3

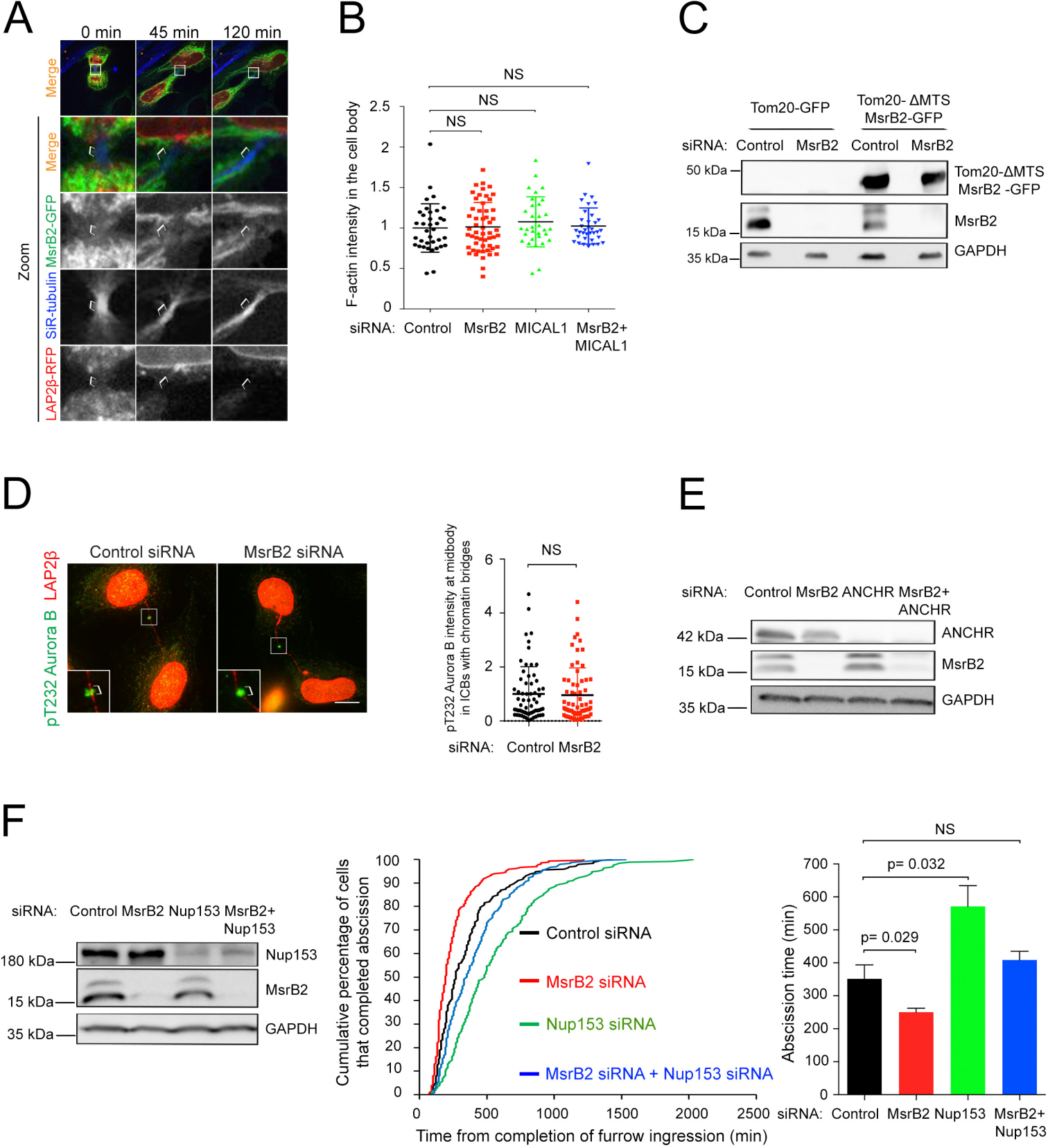
A
0 min
45 min
120 min
Merge
Zoom
Merge
MsrB2-GFP
SiR-tubulin
LAP2β-RFP
B
NS
NS
NS
F-actin intensity in the cell body
2.5
2
1.5
1
0.5
0
siRNA: Control MsrB2 MICAL1 MsrB2+ MICAL1
C
Tom20-GFP
Tom20- ΔMTS MsrB2-GFP
siRNA: Control MsrB2 Control MsrB2
50 kDa
Tom20-ΔMTS MsrB2 -GFP
15 kDa
MsrB2
35 kDa
GAPDH
D
Control siRNA
MsrB2 siRNA
pT232 Aurora B LAP2β
NS
pT232 Aurora B intensity at midbody in ICBs with chromatin bridges
6
4
2
0
siRNA: Control MsrB2
E
siRNA: Control MsrB2 ANCHR MsrB2+ ANCHR
42 kDa
ANCHR
15 kDa
MsrB2
35 kDa
GAPDH
F
siRNA: Control MsrB2 Nup153 MsrB2+ Nup153
180 kDa
Nup153
15 kDa
MsrB2
35 kDa
GAPDH
Cumulative percentage of cells that completed abscission
100
90
80
70
60
50
40
30
20
10
0
0
500
1000
1500
2000
2500
Time from completion of furrow ingression (min)
Control siRNA
MsrB2 siRNA
Nup153 siRNA
MsrB2 siRNA + Nup153 siRNA
NS
p= 0.032
p= 0.029
Abscission time (min)
700
600
500
400
300
200
100
0
siRNA: Control MsrB2 Nup153 MsrB2+ Nup153

Figure S4